Article

Immunity

Bacterial Endotoxin Activates the Coagulation Cascade through Gasdermin D-Dependent Phosphatidylserine Exposure

Graphical Abstract

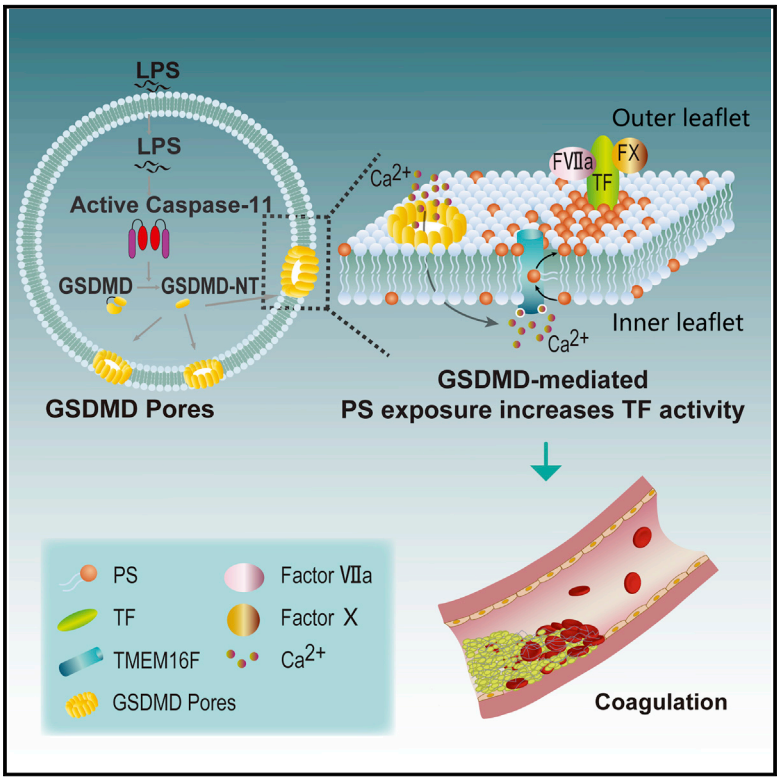

Highlights

- Deletion of caspase-11 prevents disseminated intravascular coagulation (DIC) in sepsis
- Deletion of GSDMD prevents caspase-11- and TF-mediated DIC in endotoxemia
- GSDMD deficiency inhibits endotoxin-induced TF activation by reducing PS exposure
- Activation of GSDMD by caspase-11 triggers Ca^{2+}-dependent PS exposure through TMEM16F

Authors

Xinyu Yang, Xiaoye Cheng, Yiting Tang, ..., Timothy R. Billiar, Jiahuai Han, Ben Lu

Correspondence

xybenlu@csu.edu.cn

In Brief

Excessive activation of the coagulation system by endotoxin leads to life-threatening disseminated intravascular coagulation (DIC). Yang, Cheng et al. reveal that caspase-11, a cytosolic LPS receptor, activates the coagulation cascade by enhancing the activation of tissue factor, an initiator of coagulation, through triggering the formation of gasdermin (GASMD) pores and subsequent phosphatidylserine exposure, in a manner independent of cell death.

Yang et al., 2019, Immunity *51*, 983–996
December 17, 2019
https://doi.org/10.1016/j.immuni.2019.11.005

CellPress

Immunity
Article

Bacterial Endotoxin Activates the Coagulation Cascade through Gasdermin D-Dependent Phosphatidylserine Exposure

Xinyu Yang,[1,11] Xiaoye Cheng,[1,11] Yiting Tang,[2] Xianhui Qiu,[1] Yupeng Wang,[3] Haixia Kang,[4] Jianfeng Wu,[5] Zhongtai Wang,[1] Yukun Liu,[1] Fangping Chen,[1] Xianzhong Xiao,[6,7] Nigel Mackman,[8] Timothy R. Billiar,[9] Jiahuai Han,[5] and Ben Lu[1,6,7,10,12,*]

[1]Department of Hematology and Critical Care Medicine, The 3rd Xiangya Hospital, Central South University, Changsha 410000, P.R. China
[2]Department of Physiology, School of Basic Medical Science, Central South University, Changsha, Hunan Province 410000, P.R. China
[3]National Institute of Biological Sciences, Beijing, 102206 Beijing, China
[4]Shanghai Institute of Immunology, Department of Microbiology and Immunology, Shanghai Jiao Tong University School of Medicine Shanghai 200025, P.R. China
[5]State Key Laboratory of Cellular Stress Biology, Innovation Center for Cell Signaling Network, School of Life Sciences, Xiamen University, Xiamen, Fujian, China
[6]Department of Pathophysiology, School of Basic Medical Science, Central South University, Changsha, Hunan Province 410000, P.R. China
[7]Key Laboratory of Sepsis Translational Medicine of Hunan, Central South University, Changsha, Hunan Province 410000, P.R. China
[8]Department of Medicine, University of North Carolina at Chapel Hill, Chapel Hill, NC 27599, USA
[9]Department of Surgery, University of Pittsburgh Medical Center, Pittsburgh, PA 15213, USA
[10]Senior author
[11]These authors contributed equally
[12]Lead Contact
*Correspondence: xybenlu@csu.edu.cn
https://doi.org/10.1016/j.immuni.2019.11.005

SUMMARY

Excessive activation of the coagulation system leads to life-threatening disseminated intravascular coagulation (DIC). Here, we examined the mechanisms underlying the activation of coagulation by lipopolysaccharide (LPS), the major cell-wall component of Gram-negative bacteria. We found that caspase-11, a cytosolic LPS receptor, activated the coagulation cascade. Caspase-11 enhanced the activation of tissue factor (TF), an initiator of coagulation, through triggering the formation of gasdermin D (GSDMD) pores and subsequent phosphatidylserine exposure, in a manner independent of cell death. GSDMD pores mediated calcium influx, which induced phosphatidylserine exposure through transmembrane protein 16F, a calcium-dependent phospholipid scramblase. Deletion of *Casp11*, ablation of *Gsdmd*, or neutralization of phosphatidylserine or TF prevented LPS-induced DIC. In septic patients, plasma concentrations of interleukin (IL)-1α and IL-1β, biomarkers of GSDMD activation, correlated with phosphatidylserine exposure in peripheral leukocytes and DIC scores. Our findings mechanistically link immune recognition of LPS to coagulation, with implications for the treatment of DIC.

INTRODUCTION

Coagulation is not only critical for hemostasis, but also has a role in the innate immune response to infection, acting to reduce dissemination of invading microbes (Engelmann and Massberg, 2013; Massberg et al., 2010; Niessen et al., 2008; van der Poll and Herwald, 2014). The cell membrane components of Gram-negative bacteria, including endotoxin (lipopolysaccharide [LPS]), are well-known activators of the coagulation cascade, which culminates in fibrin deposition at the site of infection (Engelmann and Massberg, 2013; Massberg et al., 2010; Pawlinski et al., 2004). Excessive activation of the coagulation cascade in endotoxemia or Gram-negative sepsis leads to disseminated intravascular coagulation (DIC), a life-threatening coagulopathy that promotes multiple organ dysfunction (Gando et al., 2013). The occurrence of DIC markedly increases the mortality in sepsis, a leading cause of mortality in hospitals (Gando et al., 2013).

Tissue factor (TF), a transmembrane glycoprotein, activates the coagulation cascade when exposed to blood by binding factor FVII/FVIIa (Chen, 2013; Grover and Mackman, 2018). LPS stimulation increases the expression of TF in myeloid and endothelial cells (Brand et al., 1991; Gregory et al., 1989; Parry and Mackman, 1998). Reducing TF expression using genetic approaches or inhibiting TF activation using monoclonal anti-TF antibodies prevents endotoxemia-induced DIC (Pawlinski et al., 2004, 2010). The activation of TF is also regulated at the post-transcriptional level. For example, the presence of phosphatidylserine in the outer leaflet of the plasma membrane markedly enhances the activity of TF (Chen, 2013; Grover and Mackman, 2018). In homeostasis, phosphatidylserine localizes exclusively to the inner leaflet

of the plasma membrane and is not in contact with the extracellular domain of TF (Chen, 2013; Grover and Mackman, 2018). Phosphatidylserine externalization leads to phosphatidylserine exposure on the outer leaflet of the plasma membrane (Nagata et al., 2016; Suzuki et al., 2010; Watanabe et al., 2018). Notably, sepsis induces robust phosphatidylserine exposure on the surface of circulating leukocytes (Zhang et al., 2016). Neutralizing exposed phosphatidylserine with lactadherin, a phosphatidylserine-binding protein, significantly attenuates coagulopathy in sepsis (Shah et al., 2012). However, there is limited understanding of the mechanisms that connect the detection of bacterial infection to phosphatidylserine exposure in sepsis.

Caspase-11, an intracellular LPS receptor, is a key component of the innate immune response to Gram-negative bacterial infection. Upon activation by LPS in the cytosol, caspase-11 cleaves gasdermin D (GSDMD) into pore-forming peptides (Ding et al., 2016; Hagar et al., 2013; Kayagaki et al., 2011, 2013, 2015; Shi et al., 2015; von Moltke et al., 2012; Wang et al., 1998). The formation of GSDMD pores either triggers pyroptosis, a lytic form of cell death that releases alarmins (e.g., IL-1α), or renders cells in a hyperactive state, in which GSDMD pores mediate IL-1 secretion without causing cell death (Evavold et al., 2018; Zanoni et al., 2016). Caspase-11 is activated in lethal endotoxemia and sepsis when hepatocyte-released high mobility group box 1 protein (HMGB1) or bacteria-released outer membrane vesicles deliver LPS into the cytosol of myeloid or endothelial cells (Deng et al., 2018; Vanaja et al., 2016). Caspase-11 activation following phagocytosis of intact bacteria requires guanylate-binding proteins, which target intracellular LPS to caspase-11 (Meunier et al., 2014; Santos et al., 2018). While caspase-11 activation contributes to host death in mouse models of endotoxemia and sepsis, the mechanisms responsible for caspase-11-mediated lethality are not well understood. Serum HMGB1 levels are correlated with the DIC scores and severity of organ failure in septic patients (Hatada et al., 2005). Together with our recent finding that HMGB1 is critical for caspase-11-dependent lethality in sepsis (Deng et al., 2018), these observations led us to postulate that caspase-11 signaling might mediate LPS-induced activation of blood coagulation.

In this study, we found that caspase-11 triggered the systemic activation of coagulation through GSDMD in endotoxemia and bacterial sepsis. GSDMD formed pores leading to calcium influx and activation of transmembrane protein 16F (TMEM16F), a calcium-dependent phospholipid scramblase that mediated phosphatidylserine exposure. This process markedly enhanced the pro-coagulant activity of TF in a manner independent of cell death. These results extend our understanding of the mechanisms that drive coagulation activation in sepsis and point to caspase-11 and its downstream signaling pathway as potential targets to prevent lethality in sepsis.

RESULTS

Caspase-11 Signaling Mediates LPS-Induced Activation of Coagulation Cascades

To test whether caspase-11 signaling mediates LPS-induced activation of coagulation cascades, wild-type (WT) and *Casp11*-deficient mice were subjected to lethal endotoxemia. The activity of the coagulation system within the liver vasculature was visualized through the systemic introduction of the internally quenched 5-FAM/QXL-520 fluorescence resonance energy transfer (FRET) substrate of thrombin during intravital microscopy. Cleavage of the substrate by thrombin led to the generation of a green fluorescence signal within the vasculature (Figure 1A; Video S1). Administration of LPS induced robust activation of intravascular thrombin generation throughout the liver microvasculature of WT but not in *Casp11*-deficient mice. Endotoxemia also induced a profound aggregation of platelets, deposition of fibrin, and occlusion of the microcirculation, which were all markedly attenuated by *Casp11* deficiency (Figures 1A–1D; Videos S1, S2, S3, and S4).

Systemic activation of the coagulation system results in consumption of fibrinogen and elevated plasma levels of D-dimer, which is formed by plasmin degradation of fibrin (Koyama et al., 2014). Circulating markers of DIC include the presence of thrombin-antithrombin (TAT) complexes formed during activation of coagulation, increases in levels of plasminogen activator inhibitor type-1 (PAI-1), an inhibitor of fibrinolysis, and platelet activation resulting in thrombocytopenia (Gando et al., 2013). *Casp11* deficiency significantly attenuated LPS-induced DIC responses (Figure 1E). Deletion of *Casp11* or pretreatment with the anticoagulant heparin markedly suppressed fibrin deposition in the livers and lungs during lethal endotoxemia, as revealed by immunohistochemical detection of fibrin deposition (Figure 1F).

Toll-like receptor 4 (TLR4) is a cell surface receptor for LPS (Chow et al., 1999; Poltorak et al., 1998) and is essential for LPS-induced caspase-11 expression (Figure S1A). Deletion of *Tlr4* prevented thrombin generation, platelets aggregation, and fibrin deposition in endotoxemia (Figure S1B). LPS challenge and cecum ligation and puncture (CLP), a clinically relevant model of polymicrobial sepsis, failed to increase plasma levels of TAT and PAI-1 in *Tlr4*-deficient mice (Figures S1C and S2D). In mice pretreated with Poly I:C, a double-stranded RNA mimetic that induces caspase-11 expression independent of TLR4 (Hagar et al., 2013; Kayagaki et al., 2013), deletion of *Casp11*, but not *Tlr4*, significantly inhibited LPS-induced thrombin generation, platelet aggregation, and fibrin deposition in the liver and prevented the increase in plasma TAT complexes, D-dimer, and PAI-1 (Figures S1C–S1F). Similar observations were obtained in mice subjected to intraperitoneal *Escherichia coli* infection or CLP, which are clinically relevant models of Gram-negative sepsis (Figures 1G–1I, S2A–S2C, and S2E). The occurrence of DIC markedly increases the mortality in septic patients (Gando et al., 2013). In line with the clinical observation, deletion of *Casp11* or pretreatment with heparin prevented organ injury and lethality in both lethal endotoxemia and bacterial sepsis (Figure S3). Together, our findings establish that caspase-11 is required for the activation of the coagulation cascade in endotoxemia and Gram-negative sepsis.

Caspase-11 Signaling Mediates LPS-Induced Activation of Coagulation Cascades through GSDMD

Caspase-11 mediates the enzymatic cleavage of GSDMD, leading to nano-pore formation in the plasma membrane and subsequent pyroptosis (Ding et al., 2016; Kayagaki et al., 2015; Shi et al., 2015). Another study reported that caspase-11 could also mediate the cleavage of pannexin-1, culminating in the activation of the purinergic receptor P2X7 (P2X7R; encoded by

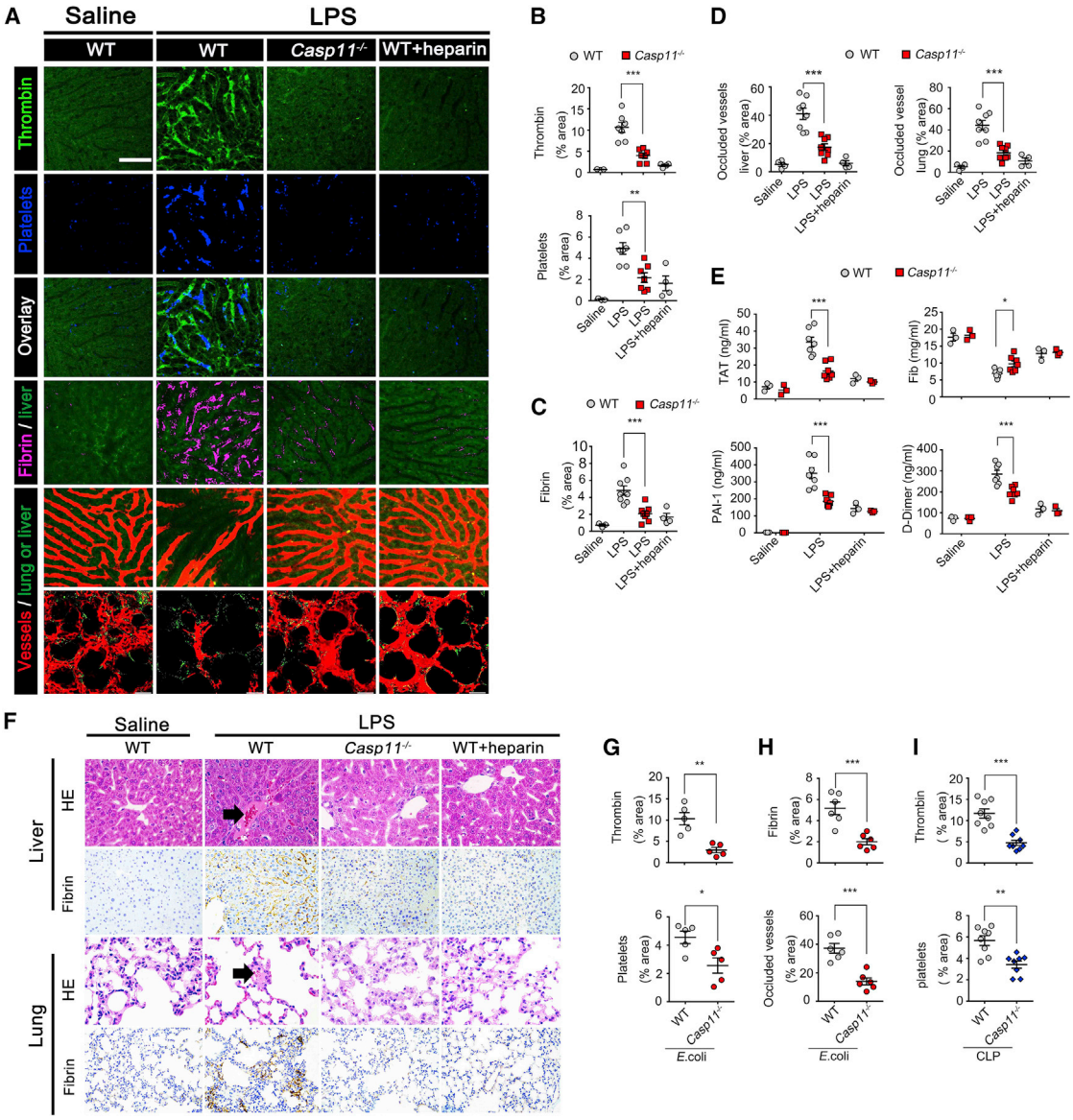

Figure 1. Caspase-11 Mediates Activation of Coagulation in Endotoxemia

(A–D) WT and *Casp11*$^{-/-}$ mice were injected intraperitoneally with LPS. Low molecular weight heparin (200 IU/kg) was administered subcutaneously 30 min before LPS injection.

(A) Representative SD-IVM images of thrombin (green), platelet adhesion (blue, AF647 anti-CD49b), fibrin deposition (dark red, AF555-fibrin), and albumin (red, AF647-albumin) within the liver or lung (multi-photon microscopy images) microvasculature at 4 h after LPS challenge. AF647-albumin (red) was regarded as a contrast material to identify perfused versus occluded vessels.

(B and C) Quantitative analysis of thrombin and platelets (B) and fibrin probe (C) fluorescence within the liver microcirculation by ImageJ software.

(D) The proportion of occluded vessels in liver and lung was quantified per field of view in endotoxemic WT versus *Casp11*$^{-/-}$ mice.

(E) Plasma concentrations of TAT complexes, PAI-1, fibrinogen, and D-dimer were measured at 8 h (the peak time of thrombin generation, data not show) in mice injected with a lethal dose of LPS (mice primed with 0.4 mg/kg LPS for 7 h and then challenged with 10 mg/kg LPS).

(F) Representative images of H&E staining and immunohistochemical (IHC) staining of fibrin in livers and lungs of endotoxemic WT versus *Casp11*$^{-/-}$ mice. Thrombus (black arrow) and fibrin deposition in liver and lung capillaries were revealed in WT mice challenged with LPS. Original magnification: H&E, 400×; IHC, 200×.

(G and H) Mice were intraperitoneally injected with *E. coli* (1×10^9 colony forming unit [CFU]) or saline. Quantitative analysis of thrombin and platelets (G) and fibrin and occluded vessels (H) probe fluorescence within the liver microcirculation after challenged with *E. coli*.

(I) Microvascular thrombin and platelets fluorescence were quantified in the mice subjected to cecum ligation and puncture (CLP).

Circles represent individual mice. *$p < 0.05$; **$p < 0.01$; ***$p < 0.001$. Data are shown as mean ± SEM, (A), (E) and (G) from three independent experiments. (B)–(D), (H), and (I) from four independent experiments, Scale bar represents 50 μm. Unpaired/two-tailed t test, one-way ANOVA, two-way ANOVA test.

See also Figures S1, S2, and S3 and Videos S1, S2, S3, and S4.

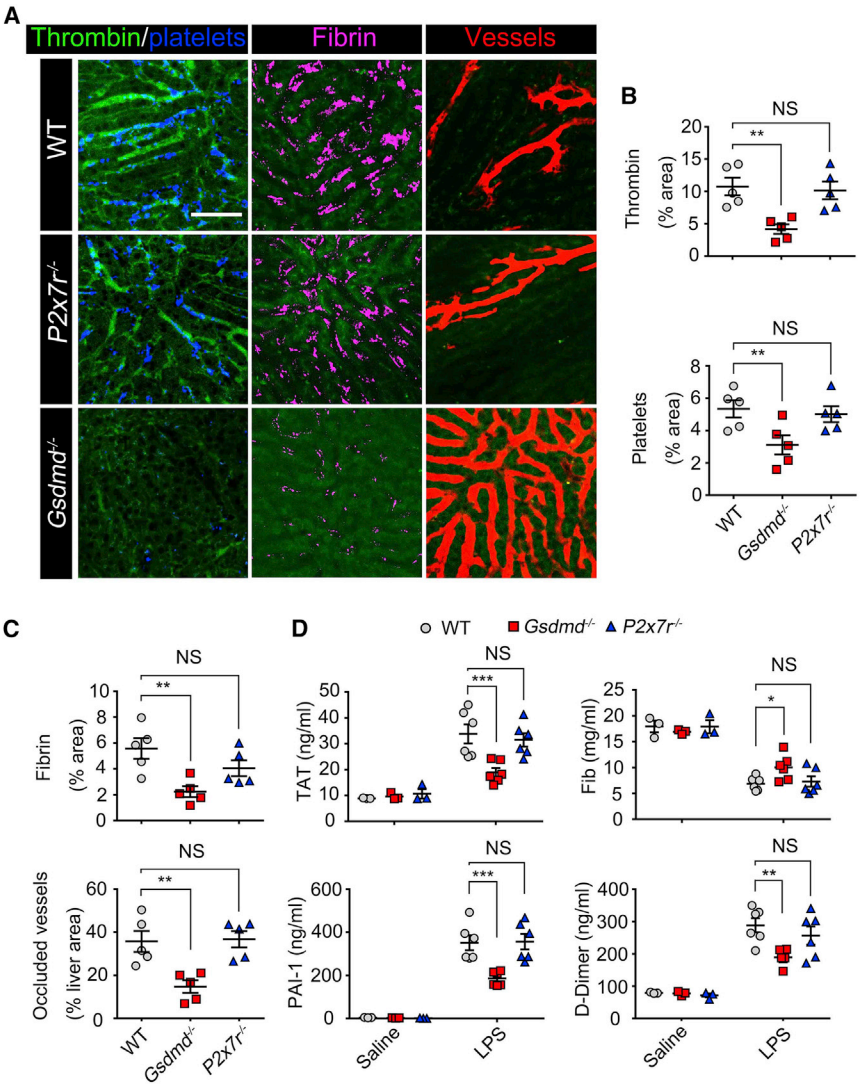

Figure 2. Caspase-11 Signaling Mediates LPS-Induced Activation of Coagulation Cascades through GSDMD but Not P2X7

(A) Representative SD-IVM images of thrombin (green), platelet adhesion (blue), fibrin (dark red), and albumin (red) within the liver microvasculature at 4 h in endotoxemic WT, *Gsdmd*$^{-/-}$, and *P2x7r*$^{-/-}$ mice.

(B and C) Quantitative analysis of thrombin and platelets (B) and fibrin fluorescence and the proportion of occluded vessels (C) in endotoxemic WT, *Gsdmd*$^{-/-}$, and *P2x7r*$^{-/-}$ mice.

(D) Plasma concentrations of TAT complexes, PAI-1, fibrinogen, and D-dimer were measured at 8 h in endotoxemic WT, *Gsdmd*$^{-/-}$, and *P2x7r*$^{-/-}$ mice. Circles represent individual mice. *p < 0.05; **p < 0.01; ***p < 0.001; NS, no statistical difference (one-way and two-way ANOVA test). Data are shown as mean ± SEM from three independent experiments. Scale bar represents 50 μm.

See also Figure S4.

P2rx7) (Yang et al., 2015). Activation of P2X7 contributes to $FeCl_3$-induced carotid artery thrombosis (Furlan-Freguia et al., 2011). To investigate the mechanisms by which caspase-11 mediates LPS-induced DIC, we subjected *Gsdmd*-deficient and *P2x7r*-deficient mice to endotoxemia. LPS challenge failed to promote thrombin generation, fibrin deposition, platelet aggregation, and microvascular occlusion within the liver in *Gsdmd*-deficient mice (Figures 2A–2C). In contrast, endotoxemia triggered thrombin generation, fibrin deposition, and platelet aggregation in *P2x7r*-deficient mice to a level similar to that seen in WT mice (Figures 2A–2C). Further, deletion of *Gsdmd*, but not *P2x7r*, prevented the increase of plasma TAT, D-dimer, and PAI-1 (Figure 2D). Together, these observations demonstrate that LPS activates the coagulation cascade and induces a DIC-like picture through GSDMD and not P2X7R.

GSDMD Increases TF Activity through Phosphatidylserine Exposure in Endotoxemia

Next, we investigated the mechanisms by which GSDMD mediates the activation of coagulation cascades during endotoxemia. In agreement with previous studies (Pawlinski et al., 2004, 2010), reducing TF expression using a genetic approach or through inhibition of TF activation using a monoclonal anti-TF antibody prevented a DIC-like picture in endotoxemia (Figures 3A–3C). *Gsdmd* deficiency significantly inhibited TF activity in endotoxemic mice (Figure 3D), indicating that GSDMD mediates TF activation in endotoxemia. GSDMD activation results in the release of IL-1α and contributes to the maturation of pro-IL-1β (Banerjee et al., 2018; Kayagaki et al., 2015). IL-1α and IL-1β have been shown to increase the expression of TF in vascular endothelial cells (Bevilacqua et al., 1984). However, deletion of *Il-1r*, the receptor for both IL-1α and IL-1β, failed to prevent LPS-induced coagulopathy (Figure S4). In line with this finding, deletion of *Gsdmd* did not affect the expression of TF in the spleen, liver, or lungs (Figures 3E and 3F). These observations prompted us to test whether GSDMD enhances TF activity at the post-transcriptional level.

Phosphatidylserine increases TF activity and enhances the assembly of cofactor-protease complexes of the coagulation cascade (Grover and Mackman, 2018). Under normal conditions, however, phosphatidylserine primarily localizes to the inner leaflet of the plasma membrane (Grover and Mackman, 2018; Nagata et al., 2016). As sepsis induces cell surface phosphatidylserine exposure in circulating leukocytes (Zhang et al., 2016), we next tested whether GSDMD mediates the phosphatidylserine exposure observed after LPS challenge. Deletion of *Gsdmd* partially reduced the phosphatidylserine externalization in peripheral leukocytes and splenocytes during endotoxemia (Figures 3G and 3H). Administration of lactadherin, a well-known phosphatidylserine-binding protein (Zhang et al., 2016), significantly attenuated coagulopathy in endotoxemia (Figures 3I and

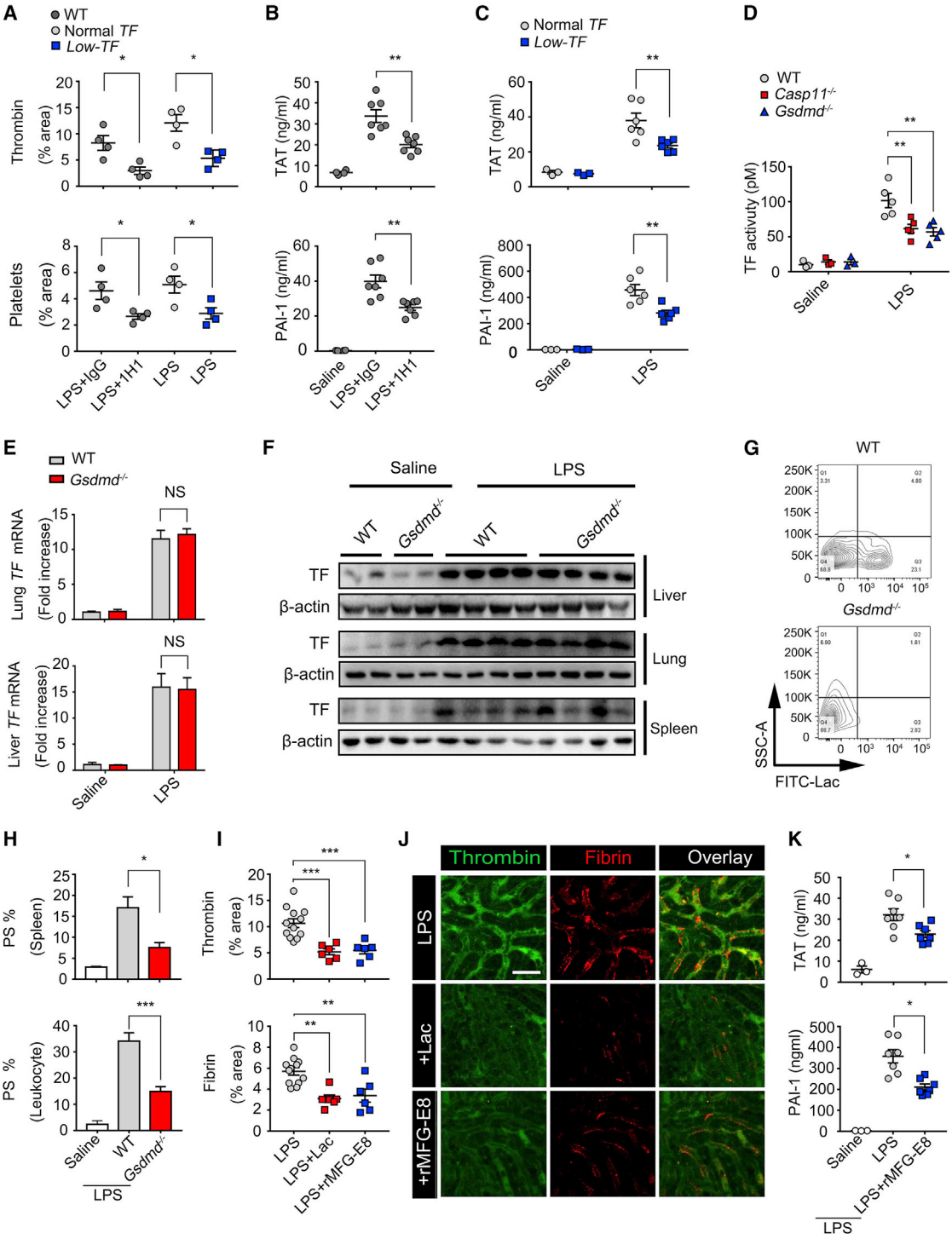

Figure 3. GSDMD Enhances the Activation of TF through Phosphatidylserine Exposure in Endotoxemia

(A) Quantitative analysis of thrombin and platelets fluorescence within the liver microvasculature in WT mice pre-treated with isotype control IgG or TF neutralizing antibody (1H1) and then challenged with LPS 30 min later (left). Quantitative analysis of above fluorescence within the liver microvasculature of normal *TF* ($mTF^{+/+}/hTF^{+}$) and *Low-TF* ($mTF^{-/-}/hTF^{+}$) mice at 4 h after administration of LPS (right).

(B) Plasma concentrations of TAT complex and PAI-1 were measured at 8 h in endotoxemic WT mice treated with isotype control IgG or TF neutralizing antibody 1H1.

(C) The plasma concentrations of TAT and PAI-1 were measured at 8 h in LPS-treated normal *TF* ($mTF^{+/+}/hTF^{+}$) and *Low-TF* ($mTF^{-/-}/hTF^{+}$) mice.

(D) Plasma TF activity were measured at 8 h in WT (HTF^{+}), *Casp11*$^{-/-}$ (HTF^{+}), and *Gsdmd*$^{-/-}$ (HTF^{+}) mice challenged with a lethal dose of LPS.

(E) *TF* mRNA expression was measured by qRT-PCR in lung and liver tissues in endotoxemic WT and *Gsdmd*$^{-/-}$ mice.

(legend continued on next page)

3J). To provide another line of evidence that phosphatidylserine exposure is critical for LPS-induced coagulopathy, we pretreated mice with milk fat globule-epidermal growth factor E8 (MFG-E8), a phosphatidylserine-binding protein (Shah et al., 2012). In line with the finding that MFG-E8 treatment improves the outcome of experimental sepsis (Shah et al., 2012), administration of MFG-E8 significantly attenuated LPS-induced coagulopathy (Figures 3I–3K). Taken together, these data indicate that GSDMD-mediated phosphatidylserine exposure is critical for the activation of coagulation cascades in endotoxemia.

GSDMD Enhances TF Activity through Phosphatidylserine Exposure *In Vitro*

We next determined whether GSDMD promotes an increase in TF activity *in vitro*. Extracellular LPS must be delivered to the cytosol in order to activate caspase-11 in cultured macrophages (Hagar et al., 2013; Kayagaki et al., 2013). Accordingly, exposure of macrophages to LPS alone failed to induce phosphatidylserine exposure and only slightly increased the procoagulant activity of TF (Figures 4A–4C). Delivery of LPS to the cytosol of macrophages using cholera toxin subunit B (CTB) induced robust phosphatidylserine exposure and TF activity in WT but not *Casp11*- or *Gsdmd*-deficient mouse macrophages (Figures 4A–4C). In line with our *in vivo* experiments (Figure 3), reducing TF expression by genetic approaches or neutralizing phosphatidylserine with lactadherin blocked LPS+CTB-induced procoagulant activity in WT mouse macrophages (Figures 4D, 4E, and 4G). Similar observations were made using MFG-E8 to neutralize phosphatidylserine (Figures 4F and 4G). Together with the finding that deletion of *Gsdmd* failed to affect LPS-induced TF expression (Figures 4H and 4I), these observations further support the notion that GSDMD promotes an increase in TF activity through phosphatidylserine exposure.

GSDMD-Mediated Calcium Influx Increases the Procoagulant Activity of TF

We then investigated the mechanisms by which GSDMD mediates phosphatidylserine exposure and increases TF activity. Upon cleavage by caspase-11, the N-terminal fragment of GSDMD forms pores with an inner diameter of 10–15 nm in the cytoplasmic membrane (Ding et al., 2016; Evavold et al., 2018). The formation of GSDMD pores allows the efflux of potassium (K^+). K^+ efflux mediates the activation of NOD-like receptor (NLR) family pyrin domain-containing 3 (NLRP3) inflammasome and the suppression of cyclic GMP-AMP synthase (cGAS) activation (Banerjee et al., 2018; Rühl and Broz, 2015). As expected, blocking K^+ efflux with KCl supplementation in cell culture medium prevented the release of IL-1β upon stimulation with CTB+LPS, indicating the blockade of the NLRP3 inflammasome (Figure S5A). In contrast, increasing extracellular concentration of KCl failed to inhibit CTB+LPS-induced phosphatidylserine exposure and TF activation (Figure 5A). GSDMD pores also mediate calcium (Ca^{2+}) influx, which triggers endosomal sorting complexes required for transport (ESCRT)-dependent membrane repair (Rühl et al., 2018). Notably, reducing Ca^{2+} concentration of the cell-culture medium markedly decreased the phosphatidylserine exposure and the TF activation upon CTB+LPS stimulation (Figure 5B). Addition of $Ca(NO_3)_2$ to the cell-culture medium dose-dependently enhanced phosphatidylserine exposure and TF activity in WT, but not *Gsdmd*-deficient, macrophages (Figure 5C). Further, chelating extracellular Ca^{2+} with BAPTA-AM or EDTA dose-dependently inhibited the phosphatidylserine exposure and TF activity (Figure 5D). These data establish that GSDMD-mediated calcium influx induces phosphatidylserine exposure and enhances TF activity.

Transmembrane protein 16F (TMEM16F) is a Ca^{2+}-dependent phospholipid scramblase, which mediates phosphatidylserine externalization in response to Ca^{2+} influx (Nagata et al., 2016; Suzuki et al., 2010; Watanabe et al., 2018). To further establish that GSDMD enhances the activation of TF through phosphatidylserine externalization, we reduced the expression of *Tmem16f* in mouse peritoneal macrophages using a small interfering RNA that targets *Tmem16f* (Figure 5E). As expected, reduced *Tmem16f* expression prevented CTB+LPS-induced phosphatidylserine exposure (Figure 5F). A recent study claims that TMEM16F is essential for GSDMD-mediated pyroptosis in genetically modified HEK293 cells (Ousingsawat et al., 2018). However, we observed that TMEM16F expression was dispensable for CTB+LPS-induced pyroptosis in mouse peritoneal macrophages (Figure 5G). In contrast, reduced *Tmem16f* expression by small interfering RNA (siRNA) markedly reduced TF activity upon CTB+LPS stimulation (Figure 5F). Further, pharmacological inhibition of TMEM16F with tannic acid (TA) or niflumic acid (NFA) significantly reduced phosphatidylserine exposure and TF activity (Figure 5H). Together, these findings demonstrate that GSDMD-mediated Ca^{2+} influx promotes TF activation, at least in part, through TMEM16F.

To test whether Ca^{2+} influx is sufficient to promote TF activation, we artificially created Ca^{2+} influx by using a Ca^{2+} ionophore (A23187). Addition of A23187 enhanced the phosphatidylserine exposure and the TF activity in *Gsdmd*-deficient macrophages (Figure 5I). Similar to GSDMD, mixed lineage kinase domain-like protein (MLKL) is able to form membrane pores that induce Ca^{2+} influx (Gong et al., 2017). This process is initiated by receptor-interacting protein kinase-3 (RIP3)-mediated MLKL phosphorylation (Sun et al., 2012). To provide further evidence that Ca^{2+} influx is sufficient to promotes TF activation, WT, *RIP3*-, or *MLKL*-deficient HT-29 cells were stimulated with tumor necrosis factor (TNF)+Smac+zVAD, which is known to activate the RIP3- MLKL pathway (Figures S5C–S5E)

(F) TF protein expression in liver, lung, and spleen in endotoxemic WT and *Gsdmd*$^{-/-}$ mice.
(G and H) Representative flow cytometry images (G) and quantitative analysis (H) of phosphatidylserine exposure labeled by lactadherin-FITC in mice splenic and peripheral blood leukocyte in endotoxemic WT and *Gsdmd*$^{-/-}$ mice.
(I and J) Mice were treated with LPS in the presence or absence of PS-neutralizing proteins (lactadherin or rMFG-E8). Thrombin (green) and fibrin (dark red) deposition were quantified (I) and representative fluorescence images of thrombin and fibrin deposition in liver microvasculature were shown (J).
(K) Plasma concentrations of TAT, PAI-1 were determined in LPS-treated mice with or without rMFG-E8.
Circles represent individual mice. *$p < 0.05$; **$p < 0.01$; ***$p < 0.001$; NS, no statistical difference (unpaired/two-tailed t test, one-way and two-way ANOVA test). Data are shown as mean ± SEM from three independent experiments. Scale bar represents 20 μm.

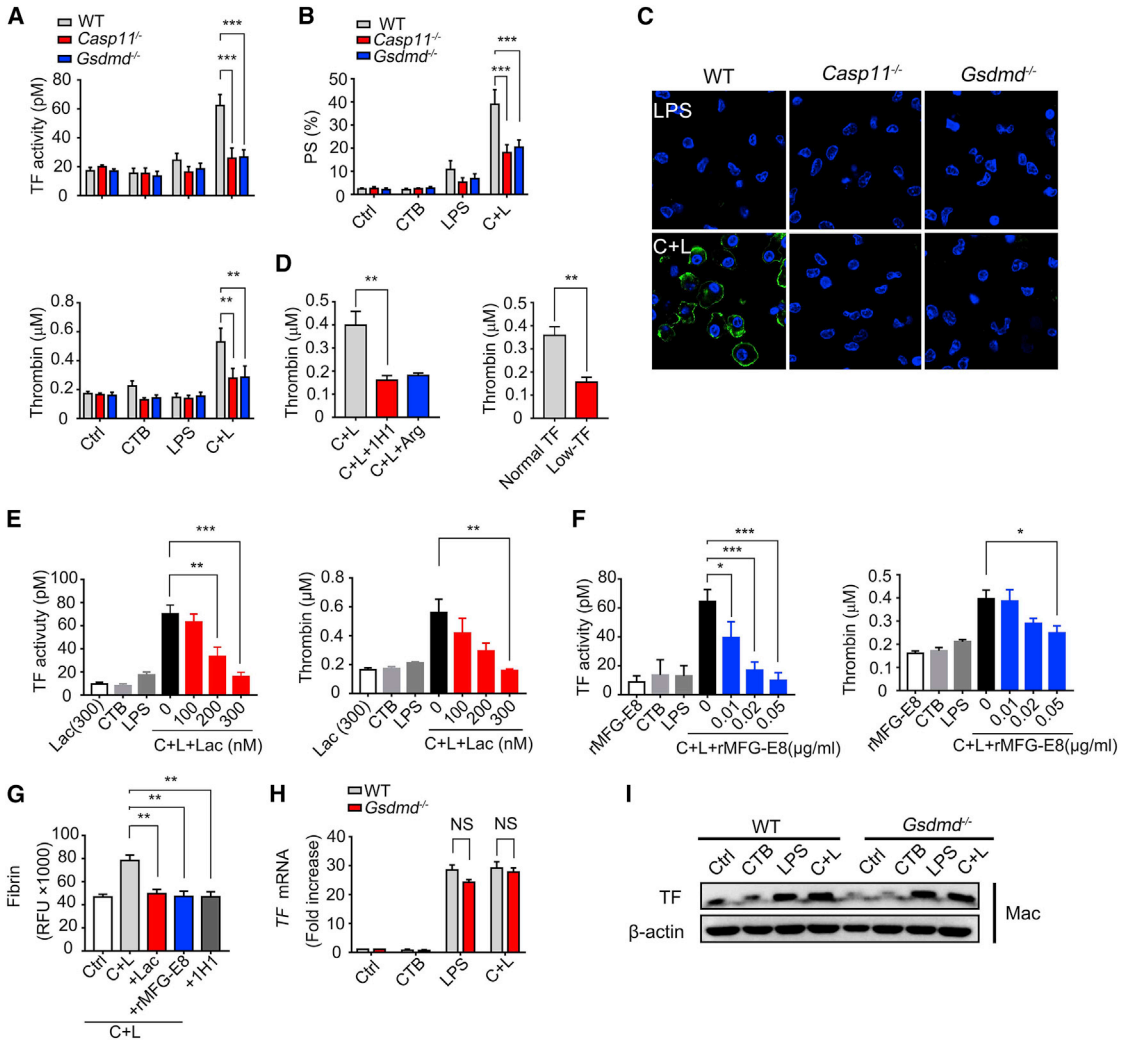

Figure 4. GSDMD Promotes the Activation of TF through Phosphatidylserine Exposure *In Vitro*

(A) Peritoneal macrophages derived from WT (*HTF*$^{+}$), *Casp11*$^{-/-}$ (*HTF*$^{+}$), and *Gsdmd*$^{-/-}$ (*HTF*$^{+}$) mice were stimulated with LPS delivered by CTB, and cell TF activity and thrombin production were assayed.

(B and C) PS exposure on macrophages with indicated stimulation was labeled by annexin V-FITC. Representative fluorescence images of PS exposure were shown (C). Microscopy images were quantified using high content screening system ScanR (Olympus) for the area percentage of cells that are positive for PS (B).

(D) Left: thrombin production in CTB+LPS-stimulated WT (*HTF*$^{+}$) macrophages with or without anti-TF 1H1 or Argatroban (thrombin inhibitor). Right: thrombin production in CTB+LPS-stimulated normal *TF* (*mTF*$^{+/+}$/*hTF*$^{+}$) and *Low-TF* (*mTF*$^{-/-}$/*hTF*$^{+}$) macrophages.

(E and F) TF activity and thrombin production were measured in WT macrophages (*HTF*$^{+}$) incubated with CTB plus LPS in the presence or absence of PS-neutralizing proteins lactadherin (E) and rMFG-E8 (F).

(G) Fibrin production in CTB+LPS-stimulated peritoneal macrophages with or without lactadherin, rMFG-E8, and anti-TF antibodies 1H1.

(H) *TF* mRNA expression in WT and *Gsdmd*$^{-/-}$ peritoneal macrophages with indicated stimulation.

(I) TF protein expression in WT and *Gsdmd*$^{-/-}$ peritoneal macrophages with indicated stimulation.

*p < 0.05; **p < 0.01; ***p < 0.001; NS, no statistical difference (unpaired/two-tailed t test, one-way ANOVA and two-way ANOVA test). Data are shown as mean ± SEM from three independent experiments. Scale bar represents 20 μm.

(Sun et al., 2012). We observed that deletion of *RIP3* or *MLKL* blocked TNF+Smac+zVAD-induced phosphatidylserine exposure and TF activation, both of which largely depended on extracellular Ca^{2+} (Figures 5J and 5K). Further, reduced *TMEM16F* expression by siRNA significantly inhibited TNF+Smac+zVAD-induced phosphatidylserine exposure and TF activation (Figure S5I). Upon cleavage by caspase-3, gasdermin E (GSMDE) is able to form membrane pores in a manner similar to GSDMD (Wang et al., 2017). To determine whether GSMDE-mediated calcium influx could enhance the phosphatidylserine exposure and TF activity, WT or *CASP3*-deficient HeLa cells stably expressing WT GSDME were stimulated with TNF+cycloheximide (CHX), which is known to activate the caspase-3-GSMDE pathway (Wang et al., 2017). After stimulation, cells expressing both CASP3 and WT GSDME displayed swelling with characteristic large bubbles from the plasma membrane and released LDH into the culture medium (Figures S5F–S5H). These responses were blocked by deletion of *CASP3* (Figures S5F–S5H). Notably,

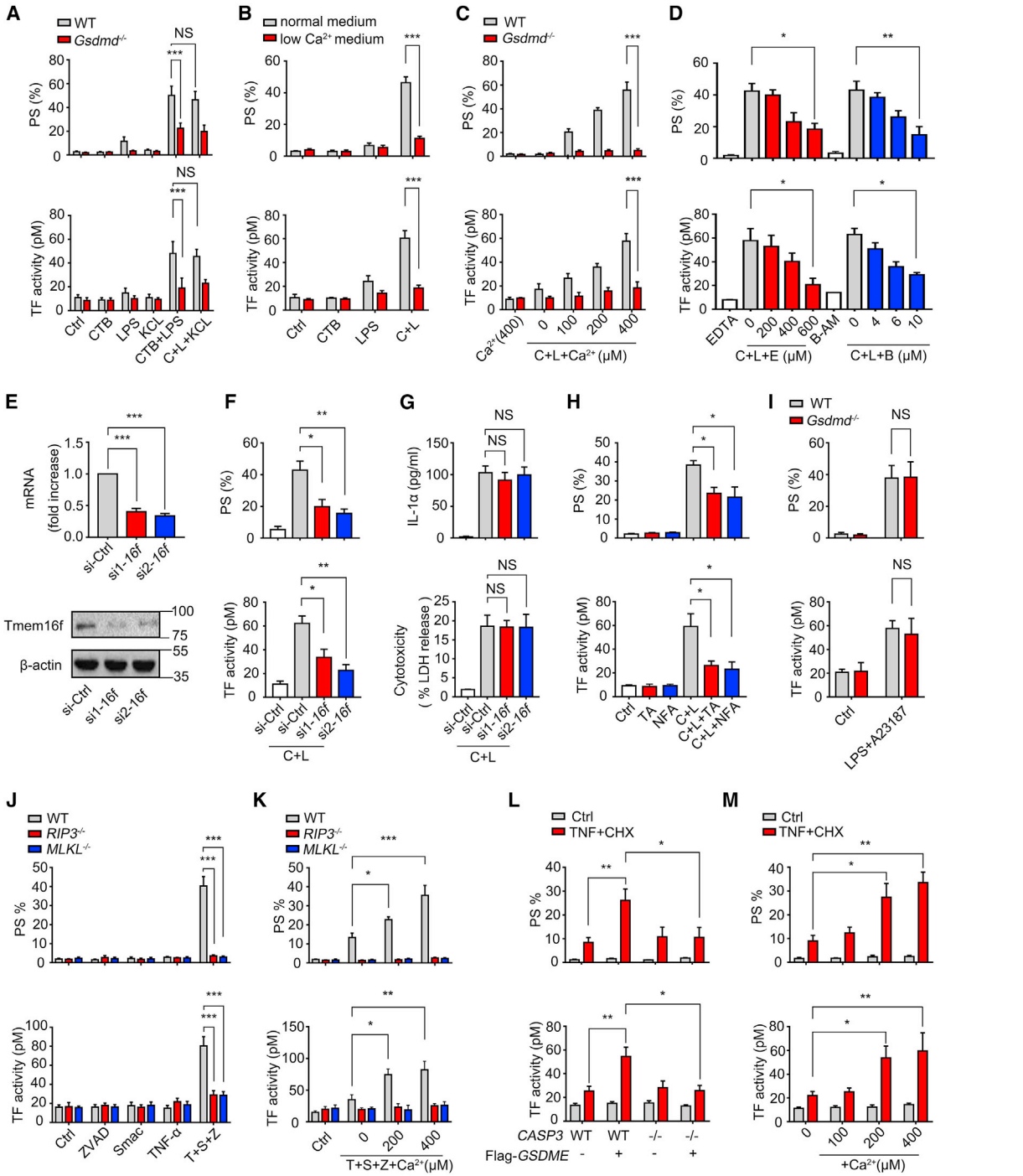

Figure 5. GSDMD-Mediated Calcium Influx Increases the Procoagulant Activity of TF

(A) WT (*HTF*$^{+}$) and *Gsdmd*$^{-/-}$ (*HTF*$^{+}$) peritoneal macrophages were stimulated with or without CTB+LPS supplemented with or without KCl. Phosphatidylserine (PS) exposure and TF activity were measured.

(B) WT (*HTF*$^{+}$) macrophages stimulated with CTB+LPS in low Ca^{2+}- containing medium or normal Ca^{2+}-containing medium. PS exposure and TF activity was measured.

(C) PS exposure and TF activity were determined in CTB+LPS-stimulated WT (*HTF*$^{+}$) and *Gsdmd*$^{-/-}$ (*HTF*$^{+}$) macrophages incubated in low Ca^{2+}- containing medium supplemented with various concentrations of Ca^{2+}.

(D) WT (*HTF*$^{+}$) macrophages were stimulated with CTB plus ultrapure LPS in normal Ca^{2+}-containing medium with or without Ca^{2+} chelators (EDTA and BAPTA-AM). PS exposure and cell TF activity were measured.

(E) Immunoblot and qPCR to detect Tmem16f in peritoneal macrophages transfected with control siRNA or *Tmem16f*-specific siRNAs.

(legend continued on next page)

deletion of *CASP3* also markedly decreased TNF+CHX-induced phosphatidylserine exposure and TF activation, both of which largely depended on extracellular Ca^{2+} (Figures 5L and 5M). Further, reduced *TMEM16F* expression by siRNA significantly inhibited TNF+CHX–induced phosphatidylserine exposure and TF activation (Figure S5I). Together, these findings further support the notion that GSDMD-mediated Ca^{2+} influx promotes TF activation, at least in part, through TMEM16F.

GSDMD Increases the Procoagulant Activity of TF-Independent of Pyroptosis

While GSDMD-mediated Ca^{2+} influx promotes TF activation, Ca^{2+} influx inhibited GSDMD-mediated pyroptosis (Figure S5B), which is in line with a previous study (Rühl et al., 2018). Thus, we reasoned that GSDMD-mediated Ca^{2+} influx might increase the procoagulant activity of TF independent of pyroptosis, which is mediated by inflammasome-dependent plasma membrane rupture. To test this, we utilized the osmoprotectant glycine to prevent pyroptosis-associated membrane rupture (Fink and Cookson, 2006). Addition of glycine to the cell-culture medium prevented LDH release but failed to affect the IL-1β release, the phosphatidylserine exposure and TF activation (Figure 6A). Similar observations were made when we utilized mannitol (Figure 6B), an agent that inhibits GSDMD-mediated cell lysis (Banerjee et al., 2018). The formation of GSDMD pores either triggers pyroptosis or renders cells in a hyperactive state, which is defined by living cells releasing IL-1 through GSDMD pores (Evavold et al., 2018; Zanoni et al., 2016). To further prove that GSDMD-mediated Ca^{2+} influx increases the procoagulant activity of TF independent of pyroptosis, LPS-primed mouse peritoneal macrophages were stimulated with the oxPAPC component PGPC or transfected with peptidoglycan (PGN), both of which are known to induce the GSDMD-dependent hyperactivation state without causing pyroptosis (Evavold et al., 2018). As expected, PGPC stimulation or PGN transfection led to IL-1β secretion and GSDMD pore formation without causing LDH release (Figures 6C and S6). Notably, PGPC stimulation or PGN transfection triggered phosphatidylserine exposure and TF activation in a Ca^{2+}- and GSDMD-dependent manner (Figures 6C and 6D). Further, reduced *Tmem16f* significantly inhibited PGPC- or PGN-induced phosphatidylserine exposure and TF activation (Figure 6E). Collectively, these findings establish that GSDMD-mediated Ca^{2+} influx increases the procoagulant activity of TF independent of pyroptosis.

Biomarkers of GSDMD Activation Are Associated with the Development of DIC in Septic Patients

Activation of GSDMD mediates the release of IL-1α and IL-1β in sepsis (Banerjee et al., 2018; Kayagaki et al., 2015). To determine if the biomarkers of GSDMD activation are associated with the development of DIC in septic patients, we measured plasma levels of IL-1α and IL-1β in 51 septic patients (patient characteristics are shown in Table S1). Plasma levels of IL-1α and IL-1β significantly correlated with TAT complexes, PAI-1, DIC score, and phosphatidylserine externalization in peripheral leukocytes (Figures 7A, 7B, S7A, and S7B). We also observed that plasma levels of IL-1α and IL-1β in sepsis non-survivors were significantly higher than those measured in survivors (Figure 7C). To exclude the possibility that elevated plasma levels of IL-1α and IL-1β simply reflect enhanced global inflammatory responses, we measured the plasma levels of IL-6 and C-reactive protein (CRP). In contrast to plasma IL-1α and IL-1β levels, plasma concentrations of IL-6 and CRP did not significantly correlate with concentrations of TAT, PAI-1, DIC scores, or phosphatidylserine externalization (Figures 7D, 7E, and S7C). These data further support the notion that GSDMD activation contributes to the development of DIC.

DISCUSSION

Caspase-11-mediated pyroptosis destroys the intracellular niche for cytosol-invasive bacteria and activates local anti-microbial immune defenses by releasing pro-inflammatory cytokines, including IL-1α and IL-1β (Aachoui et al., 2013; Man et al., 2016). In this study, we showed that caspase-11- and GSDMD-mediated calcium influx rather than pyroptosis activated the coagulation cascade in response to LPS. It was previously believed that pyroptotic cell death is required for the release of IL-1 family cytokines. However, recent reports reveal that GSDMD pores serve as conduits for the secretion of IL-1 family cytokines in viable macrophages (Evavold et al., 2018; Zanoni et al., 2016). This process is termed the hyperactivation of macrophages. As shown in this study, GSDMD pores formation promoted coagulation through calcium influx in viable macrophages. Thus, the hyperactivation of macrophages not only

(F and G) PS exposure, TF activity (F), IL-1α, and LDH (G) were measured in CTB+LPS-treated WT (*HTF*$^{+}$) peritoneal macrophages transfected with control siRNA or *Tmem16f*-specific siRNAs.

(H) WT (*HTF*$^{+}$) macrophages were treated with CTB plus ultrapure LPS with or without different TMEM16F inhibitors of tannic acid (TA) or niflumic acid (NFA). PS exposure and TF activity were detected.

(I) PS exposure and TF activity were assayed in WT (*HTF*$^{+}$) and *Gsdmd*$^{-/-}$ (*HTF*$^{+}$) macrophages primed with LPS then stimulated with calcium ionophore A23187.

(J) PS exposure and TF activity were measured in WT, *RIP3*$^{-/-}$, and *MLKL*$^{-/-}$ HT-29 cells incubated with conventional necroptotic stimuli: TNF-α (T, 30 ng/mL)+Smac (S,1 μM)+ZVAD (Z, 20 μM).

(K) PS exposure and TF activity were measured in T+S+Z-stimulated WT, *RIP3*$^{-/-}$, and *MLKL*$^{-/-}$ HT-29 cells in low Ca^{2+}- containing medium supplemented with various concentrations of Ca^{2+}.

(L) PS exposure and TF activity were measured in TNF-α+cycloheximide (CHX)-stimulated WT or *CASP3*$^{-/-}$ HeLa cells stably expressing WT GSDME (Flag-GSDME) or a vector. Above HeLa cells were all deficient in *GSDMD*.

(M) PS exposure and TF activity were measured in TNF-α+CHX-stimulated WT HeLa (*GSDMD*$^{-/-}$) cells stably expressing Flag-GSDME in low Ca^{2+}- containing medium supplemented with various concentrations of Ca^{2+}.

*$p < 0.05$; **$p < 0.01$; ***$p < 0.001$; NS, no statistical difference (one-way ANOVA and two-way ANOVA test). Data are represented as mean ± SEM from three independent experiments.

See also Figure S5.

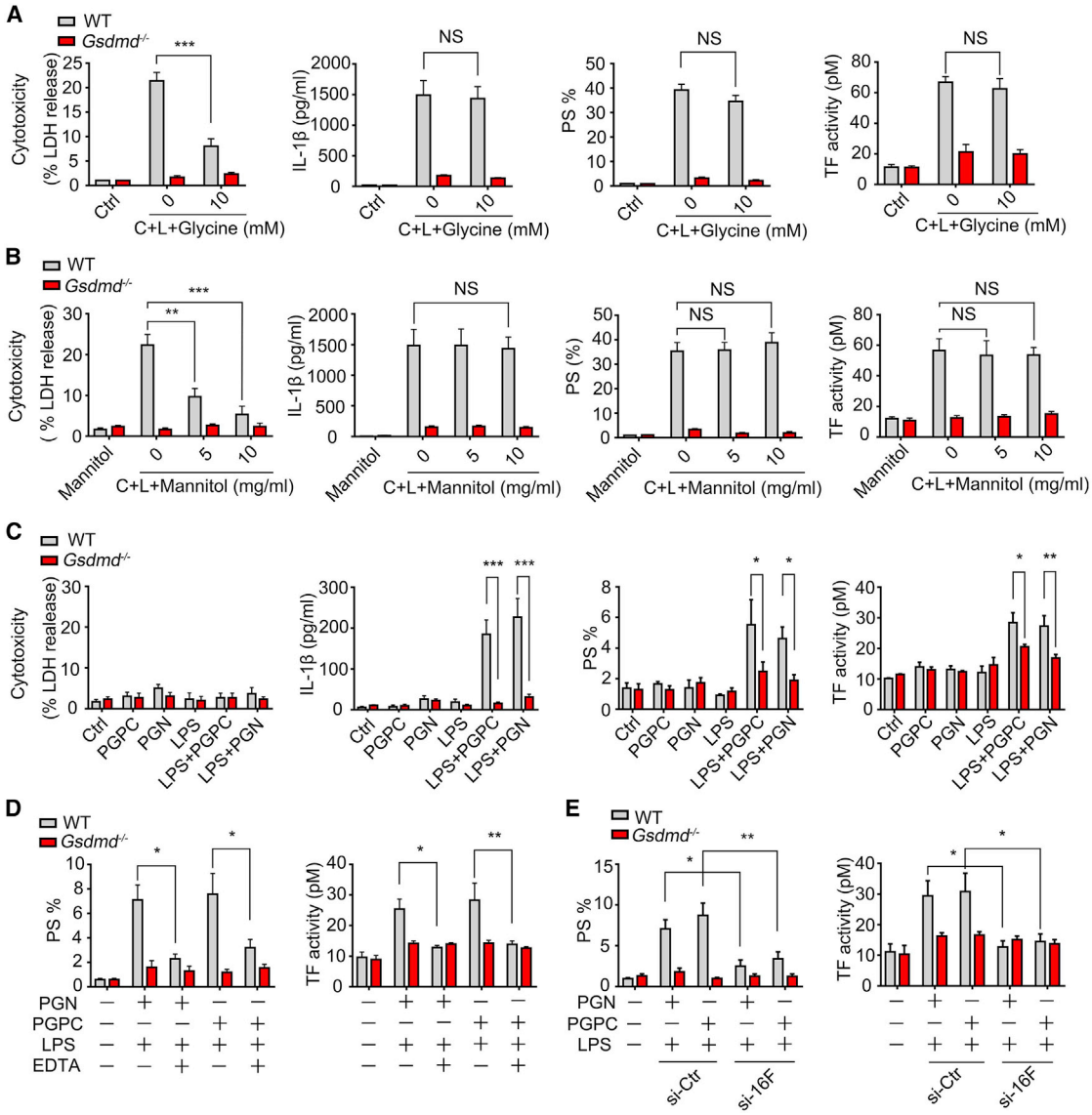

Figure 6. GSDMD Increases the Procoagulant Activity of TF Independent of Pyroptosis

(A) LDH release, IL-1β secretion, PS exposure, and TF activity were measured in WT and *Gsdmd*$^{-/-}$ peritoneal macrophages stimulated with CTB+LPS in the presence or the absence of glycine.

(B) LDH release, IL-1β secretion, PS exposure, and TF activity were measured in WT and *Gsdmd*$^{-/-}$ peritoneal macrophages stimulated with CTB+LPS in the presence or the absence of mannitol.

(C) LDH release, IL-1β secretion, PS exposure, and TF activity in WT and *Gsdmd*$^{-/-}$ peritoneal macrophages stimulated with LPS+PGPC or transfected with PGN after LPS priming.

(D) PS exposure and TF activity were measured in WT and *Gsdmd*$^{-/-}$ peritoneal macrophages pre-treated with EDTA then stimulated with LPS+ PGPC or transfected with PGN.

(E) PS exposure and TF activity were measured in LPS+ PGPC- or PGN-treated peritoneal macrophages transfected with *Tmem16f* siRNA or control scramble siRNA.

See also Figure S6.

induces the secretion of IL-1 family cytokines but also promotes coagulation. Coagulation activation is part of the innate immune system effort to trap microbes in the microvasculature. It is conceivable that activation of caspase-11 by LPS might prevent dissemination of Gram-negative bacteria through triggering the coagulation cascade. However, when local bacterial infection escalates into sepsis, this immune-thrombotic response becomes widespread and leads to life-threatening DIC (Gando et al., 2013; Koyama et al., 2014).

Mechanistically, our findings indicated that caspase-11-GSDMD signaling induced coagulation, at least in part, through the phosphatidylserine externalization. This was critical for the activation of TF and the assembly of cofactor-protease complexes of the coagulation cascade. In line with a previous

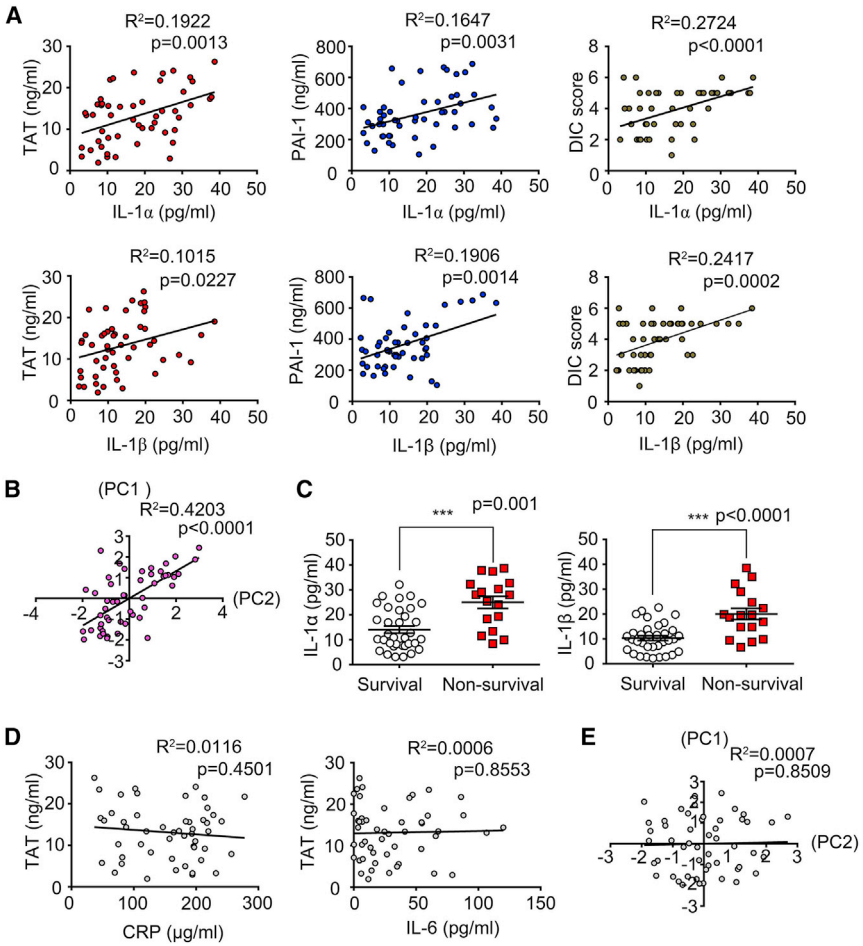

Figure 7. Biomarkers of GSDMD Activation Are Associated with the Development of DIC in Septic Patients

(A) The plasma concentrations of IL-1α and IL-1β significantly correlated with the concentrations of TAT and PAI-1, and overt DIC score in patients with sepsis.

(B) Principal component analysis (PCA) of the correlation between biomarkers of GSDMD activation and coagulation parameters (PC1: TAT, PAI-1, and DIC score; PC2: IL-1α and IL-1β).

(C) Plasma concentrations of IL-1α and IL-1β were detected in septic non-survivors and survivors, respectively.

(D) The plasma concentrations of CRP and IL-6 did not correlate with the concentration of TAT in patients with sepsis.

(E) Principal component analysis (PCA) of the correlation between biomarkers of global inflammation and coagulation parameters (PC1: TAT, PAI-1, and DIC score; PC2: CRP and IL-6).

See also Figure S7 and Table S1.

work (Pawlinski et al., 2004), we showed that reducing TF expression greatly attenuated LPS-induced DIC. In addition to phosphatidylserine externalization and TF activation, the impaired anticoagulant pathways or alterations in the regulatory angiopoietin-1/Tie2 signaling resulting from endothelial dysfunction might also contribute to the pathogenesis of DIC (Higgins et al., 2018; Levi et al., 2003). Intriguingly, selective deletion of *Casp11* in endothelial cells confers protection against lethal endotoxemia (Cheng et al., 2017). These findings raise an intriguing possibility that caspase-11-mediated pyroptosis or dysfunction of endothelial cells might also promote DIC by compromising anticoagulant pathways and/or inducing phosphatidylserine externalization.

Caspase-11-dependent pyroptosis leads to an eicosanoid storm via cyclooxygenase (COX)-1 in peritoneal macrophages during endotoxemia and bacterial sepsis (Deng et al., 2018; Hagar et al., 2013). This process may result in a vascular fluid leak into the intestine and peritoneal cavity (von Moltke et al., 2012). Pharmacological inhibition of COX-1 confers significant protection against lethal endotoxemia (Deng et al., 2018). It has been postulated that eicosanoid storm-mediated vascular leakage is a major cause of septic shock. However, septic shock is defined by sepsis with fluid resuscitation-irreversible hypotension (Seymour et al., 2016). Loss of vascular fluid alone is not sufficient to explain pathophysiology of septic shock (Seymour et al., 2016). Instead, the accumulated clinical evidence indicates that coagulopathy, especially DIC, is a major contributor to fluid resuscitation-irreversible shock and multiple organ dysfunction in sepsis (Gando et al., 2013; Koyama et al., 2014). The occurrence of DIC increases the mortality of sepsis 3-fold (Gando et al., 2013; Koyama et al., 2014). In line with clinical observations, pretreatment with the anticoagulant heparin prevents organ injuries and lethality in experimental sepsis. It is noteworthy that COX-1-dependent eicosanoid production is critical for platelet activation and aggregation (Schrör, 1997), which importantly contributes to the development of DIC. In line with this, we found that deletion of *Casp11* or *Gsdmd* prevented platelet aggregation within the vasculature in endotoxemia. Thus, our findings provide novel insights into how the caspase-11-GSDMD signaling contributes to the sepsis-induced lethality and might open a new avenue to treat sepsis-associated DIC.

STAR★METHODS

Detailed methods are provided in the online version of this paper and include the following:

- KEY RESOURCES TABLE
- LEAD CONTACT AND MATERIALS AVAILABILITY
- EXPERIMENTAL MODEL AND SUBJECT DETAILS
  - Mouse studies
  - LPS-induced Endotoxemia and E.coli-induced peritonitis
  - Caecal Ligation and Puncture (CLP)
  - Cell lines culture and stimulation
  - Macrophage cultures and stimulation
  - Clinical Human Samples

- METHOD DETAILS
  - Preparation of the Liver and Lung for Intravital Microscopy
  - Spinning Disk Confocal Intravital Microscopy Analysis
  - Multiphoton Laser Scanning Confocal Intravital Microscopy Analysis
  - ELISA, Biochemical Assays and LDH Assay
  - Liver and Lung Histology
  - Tissue factor activity, thrombin and fibrin assays
  - Measurement of PS exposure
  - Immunoblot analysis and qRT–PCR
- QUANTIFICATION AND STATISTICAL ANALYSIS
- DATA AND CODE AVAILABILITY

SUPPLEMENTAL INFORMATION

Supplemental Information can be found online at https://doi.org/10.1016/j.immuni.2019.11.005.

ACKNOWLEDGMENTS

We thank Xiangyu Wang for her excellent technical support. We thank Qianqian Xue for managing mouse colonies and research assistance. We thank Professor Feng Shao for providing key cell lines. We thank Professor Dongsheng Cao for the principal component analysis. This study was supported by the National key scientific project 2015CB910700 (to B.L.), National Natural Science Foundation of China (81930059 and 81470345 to B.L. and 81971893 to Y.T.), and Innovation-driven scientific project of CSU (to B.L.).

AUTHOR CONTRIBUTIONS

B.L. conceived the project, designed the experiments, and wrote the manuscript. X.Y., X.C., Y.L., X.Q., Z.W., Y.W., H.K., and J.W. did the experiments. T.R.B., J.H., Y.T., F.C., and X.X. commented and edited the manuscript. J.H. and N.M. provided key reagents and transgenic mice. X.Y. and X.C. analyzed the data and made the figures.

DECLARATION OF INTERESTS

The authors declare no competing interests.

Received: April 30, 2019
Revised: September 11, 2019
Accepted: November 8, 2019
Published: December 10, 2019

REFERENCES

Aachoui, Y., Leaf, I.A., Hagar, J.A., Fontana, M.F., Campos, C.G., Zak, D.E., Tan, M.H., Cotter, P.A., Vance, R.E., Aderem, A., and Miao, E.A. (2013). Caspase-11 protects against bacteria that escape the vacuole. Science *339*, 975–978.

Banerjee, I., Behl, B., Mendonca, M., Shrivastava, G., Russo, A.J., Menoret, A., Ghosh, A., Vella, A.T., Vanaja, S.K., Sarkar, S.N., et al. (2018). Gasdermin D Restrains Type I Interferon Response to Cytosolic DNA by Disrupting Ionic Homeostasis. Immunity *49*, 413–426.

Bevilacqua, M.P., Pober, J.S., Majeau, G.R., Cotran, R.S., and Gimbrone, M.A., Jr. (1984). Interleukin 1 (IL-1) induces biosynthesis and cell surface expression of procoagulant activity in human vascular endothelial cells. J. Exp. Med. *160*, 618–623.

Brand, K., Fowler, B.J., Edgington, T.S., and Mackman, N. (1991). Tissue factor mRNA in THP-1 monocytic cells is regulated at both transcriptional and posttranscriptional levels in response to lipopolysaccharide. Mol. Cell Biol. *11*, 4732–4738.

Cao, M., Li, T., He, Z., Wang, L., Yang, X., Kou, Y., Zou, L., Dong, X., Novakovic, V.A., Bi, Y., et al. (2017). Promyelocytic extracellular chromatin exacerbates coagulation and fibrinolysis in acute promyelocytic leukemia. Blood *129*, 1855–1864.

Chen, V.M. (2013). Tissue factor de-encryption, thrombus formation, and thiol-disulfide exchange. Sem. Thromb. Hemost. *39*, 40–47.

Cheng, K.T., Xiong, S., Ye, Z., Hong, Z., Di, A., Tsang, K.M., Gao, X., An, S., Mittal, M., Vogel, S.M., et al. (2017). Caspase-11-mediated endothelial pyroptosis underlies endotoxemia-induced lung injury. J. Clin. Invest. *127*, 4124–4135.

Chow, J.C., Young, D.W., Golenbock, D.T., Christ, W.J., and Gusovsky, F. (1999). Toll-like receptor-4 mediates lipopolysaccharide-induced signal transduction. J. Biol. Chem. *274*, 10689–10692.

Deng, M., Tang, Y., Li, W., Wang, X., Zhang, R., Zhang, X., Zhao, X., Liu, J., Tang, C., Liu, Z., et al. (2018). The Endotoxin Delivery Protein HMGB1 Mediates Caspase-11-Dependent Lethality in Sepsis. Immunity *49*, 740–753.

Ding, J., Wang, K., Liu, W., She, Y., Sun, Q., Shi, J., Sun, H., Wang, D.C., and Shao, F. (2016). Pore-forming activity and structural autoinhibition of the gasdermin family. Nature *535*, 111–116.

Engelmann, B., and Massberg, S. (2013). Thrombosis as an intravascular effector of innate immunity. Nat. Rev. Immunol. *13*, 34–45.

Evavold, C.L., Ruan, J., Tan, Y., Xia, S., Wu, H., and Kagan, J.C. (2018). The Pore-Forming Protein Gasdermin D Regulates Interleukin-1 Secretion from Living Macrophages. Immunity *48*, 35–44.

Fink, S.L., and Cookson, B.T. (2006). Caspase-1-dependent pore formation during pyroptosis leads to osmotic lysis of infected host macrophages. Cell. Microbiol. *8*, 1812–1825.

Furlan-Freguia, C., Marchese, P., Gruber, A., Ruggeri, Z.M., and Ruf, W. (2011). P2X7 receptor signaling contributes to tissue factor-dependent thrombosis in mice. J. Clin. Invest. *121*, 2932–2944.

Gando, S., Saitoh, D., Ishikura, H., Ueyama, M., Otomo, Y., Oda, S., Kushimoto, S., Tanjoh, K., Mayumi, T., Ikeda, T., et al.; Japanese Association for Acute Medicine Disseminated Intravascular Coagulation (JAAM DIC) Study Group for the JAAM DIC Antithrombin Trial (JAAMDICAT) (2013). A randomized, controlled, multicenter trial of the effects of antithrombin on disseminated intravascular coagulation in patients with sepsis. Crit. Care *17*, R297.

Gong, Y.N., Guy, C., Olauson, H., Becker, J.U., Yang, M., Fitzgerald, P., Linkermann, A., and Green, D.R. (2017). ESCRT-III Acts Downstream of MLKL to Regulate Necroptotic Cell Death and Its Consequences. Cell *169*, 286–300.

Gregory, S.A., Morrissey, J.H., and Edgington, T.S. (1989). Regulation of tissue factor gene expression in the monocyte procoagulant response to endotoxin. Mol. Cell Biol. *9*, 2752–2755.

Grover, S.P., and Mackman, N. (2018). Tissue Factor: An Essential Mediator of Hemostasis and Trigger of Thrombosis. Arterioscler. Thromb. Vasc. Biol. *38*, 709–725.

Hagar, J.A., Powell, D.A., Aachoui, Y., Ernst, R.K., and Miao, E.A. (2013). Cytoplasmic LPS activates caspase-11: implications in TLR4-independent endotoxic shock. Science *341*, 1250–1253.

Hatada, T., Wada, H., Nobori, T., Okabayashi, K., Maruyama, K., Abe, Y., Uemoto, S., Yamada, S., and Maruyama, I. (2005). Plasma concentrations and importance of High Mobility Group Box protein in the prognosis of organ failure in patients with disseminated intravascular coagulation. Thromb. Haemost. *94*, 975–979.

He, W.T., Wan, H., Hu, L., Chen, P., Wang, X., Huang, Z., Yang, Z.H., Zhong, C.Q., and Han, J. (2015). Gasdermin D is an executor of pyroptosis and required for interleukin-1β secretion. Cell Res. *25*, 1285–1298.

Higgins, S.J., De Ceunynck, K., Kellum, J.A., Chen, X., Gu, X., Chaudhry, S.A., Schulman, S., Libermann, T.A., Lu, S., Shapiro, N.I., et al. (2018). Tie2 protects the vasculature against thrombus formation in systemic inflammation. J. Clin. Invest. *128*, 1471–1484.

Hui, K.Y., Haber, E., and Matsueda, G.R. (1983). Monoclonal antibodies to a synthetic fibrin-like peptide bind to human fibrin but not fibrinogen. Science *222*, 1129–1132.

Jolliffe, I.T., and Cadima, J. (2016). Principal component analysis: a review and recent developments. Philosophical transactions. Philos. Trans. A Math. Phys. Eng. Sci. *374*, 20150202.

Kayagaki, N., Stowe, I.B., Lee, B.L., O'Rourke, K., Anderson, K., Warming, S., Cuellar, T., Haley, B., Roose-Girma, M., Phung, Q.T., et al. (2015). Caspase-11 cleaves gasdermin D for non-canonical inflammasome signalling. Nature *526*, 666–671.

Kayagaki, N., Warming, S., Lamkanfi, M., Vande Walle, L., Louie, S., Dong, J., Newton, K., Qu, Y., Liu, J., Heldens, S., et al. (2011). Non-canonical inflammasome activation targets caspase-11. Nature *479*, 117–121.

Kayagaki, N., Wong, M.T., Stowe, I.B., Ramani, S.R., Gonzalez, L.C., Akashi-Takamura, S., Miyake, K., Zhang, J., Lee, W.P., Muszyński, A., et al. (2013). Noncanonical inflammasome activation by intracellular LPS independent of TLR4. Science *341*, 1246–1249.

Kirchhofer, D., Moran, P., Bullens, S., Peale, F., and Bunting, S. (2005). A monoclonal antibody that inhibits mouse tissue factor function. J. Thromb. Haemost. *3*, 1098–1099.

Kolaczkowska, E., Jenne, C.N., Surewaard, B.G., Thanabalasuriar, A., Lee, W.Y., Sanz, M.J., Mowen, K., Opdenakker, G., and Kubes, P. (2015). Molecular mechanisms of NET formation and degradation revealed by intravital imaging in the liver vasculature. Nat. Commun. *6*, 6673.

Koyama, K., Madoiwa, S., Nunomiya, S., Koinuma, T., Wada, M., Sakata, A., Ohmori, T., Mimuro, J., and Sakata, Y. (2014). Combination of thrombin-antithrombin complex, plasminogen activator inhibitor-1, and protein C activity for early identification of severe coagulopathy in initial phase of sepsis: a prospective observational study. Crit. Care *18*, R13.

Lefrançais, E., Ortiz-Muñoz, G., Caudrillier, A., Mallavia, B., Liu, F., Sayah, D.M., Thornton, E.E., Headley, M.B., David, T., Coughlin, S.R., et al. (2017). The lung is a site of platelet biogenesis and a reservoir for haematopoietic progenitors. Nature *544*, 105–109.

Levi, M., Dörffler-Melly, J., Reitsma, P., Buller, H., Florquin, S., van der Poll, T., and Carmeliet, P. (2003). Aggravation of endotoxin-induced disseminated intravascular coagulation and cytokine activation in heterozygous protein-C-deficient mice. Blood *101*, 4823–4827.

Lu, B., Nakamura, T., Inouye, K., Li, J., Tang, Y., Lundbäck, P., Valdes-Ferrer, S.I., Olofsson, P.S., Kalb, T., Roth, J., et al. (2012). Novel role of PKR in inflammasome activation and HMGB1 release. Nature *488*, 670–674.

Man, S.M., Karki, R., Sasai, M., Place, D.E., Kesavardhana, S., Temirov, J., Frase, S., Zhu, Q., Malireddi, R.K.S., Kuriakose, T., et al. (2016). IRGB10 Liberates Bacterial Ligands for Sensing by the AIM2 and Caspase-11-NLRP3 Inflammasomes. Cell *167*, 382–396.

Massberg, S., Grahl, L., von Bruehl, M.L., Manukyan, D., Pfeiler, S., Goosmann, C., Brinkmann, V., Lorenz, M., Bidzhekov, K., Khandagale, A.B., et al. (2010). Reciprocal coupling of coagulation and innate immunity via neutrophil serine proteases. Nat. Med. *16*, 887–896.

Meunier, E., Dick, M.S., Dreier, R.F., Schurmann, N., Kenzelmann Broz, D., Warming, S., Roose-Girma, M., Bumann, D., Kayagaki, N., Takeda, K., et al. (2014). Caspase-11 activation requires lysis of pathogen-containing vacuoles by IFN-induced GTPases. Nature *509*, 366–370.

Nagata, S., Suzuki, J., Segawa, K., and Fujii, T. (2016). Exposure of phosphatidylserine on the cell surface. Cell Death Differ. *23*, 952–961.

Niessen, F., Schaffner, F., Furlan-Freguia, C., Pawlinski, R., Bhattacharjee, G., Chun, J., Derian, C.K., Andrade-Gordon, P., Rosen, H., and Ruf, W. (2008). Dendritic cell PAR1-S1P3 signalling couples coagulation and inflammation. Nature *452*, 654–658.

Ousingsawat, J., Wanitchakool, P., Schreiber, R., and Kunzelmann, K. (2018). Contribution of TMEM16F to pyroptotic cell death. Cell Death Dis. *9*, 300.

Parry, G.C., Erlich, J.H., Carmeliet, P., Luther, T., and Mackman, N. (1998). Low levels of tissue factor are compatible with development and hemostasis in mice. J. Clin. Invest. *101*, 560–569.

Parry, G.C., and Mackman, N. (1998). NF-κB Mediated Transcription in Human Monocytic Cells and Endothelial Cells. Trends Cardiovasc. Med. *8*, 138–142.

Pawlinski, R., Pedersen, B., Schabbauer, G., Tencati, M., Holscher, T., Boisvert, W., Andrade-Gordon, P., Frank, R.D., and Mackman, N. (2004). Role of tissue factor and protease-activated receptors in a mouse model of endotoxemia. Blood *103*, 1342–1347.

Pawlinski, R., Tencati, M., Holscher, T., Pedersen, B., Voet, T., Tilley, R.E., Marynen, P., and Mackman, N. (2007). Role of cardiac myocyte tissue factor in heart hemostasis. J. Thromb. Haemost. *5*, 1693–1700.

Pawlinski, R., Wang, J.G., Owens, A.P., 3rd, Williams, J., Antoniak, S., Tencati, M., Luther, T., Rowley, J.W., Low, E.N., Weyrich, A.S., and Mackman, N. (2010). Hematopoietic and nonhematopoietic cell tissue factor activates the coagulation cascade in endotoxemic mice. Blood *116*, 806–814.

Poltorak, A., He, X., Smirnova, I., Liu, M.Y., Van Huffel, C., Du, X., Birdwell, D., Alejos, E., Silva, M., Galanos, C., et al. (1998). Defective LPS signaling in C3H/HeJ and C57BL/10ScCr mice: mutations in Tlr4 gene. Science *282*, 2085–2088.

Risom, T., Langer, E.M., Chapman, M.P., Rantala, J., Fields, A.J., Boniface, C., Alvarez, M.J., Kendsersky, N.D., Pelz, C.R., Johnson-Camacho, K., et al. (2018). Differentiation-state plasticity is a targetable resistance mechanism in basal-like breast cancer. Nat. Commun. *9*, 3815.

Rittirsch, D., Huber-Lang, M.S., Flierl, M.A., and Ward, P.A. (2009). Immunodesign of experimental sepsis by cecal ligation and puncture. Nat. Protoc. *4*, 31–36.

Rühl, S., and Broz, P. (2015). Caspase-11 activates a canonical NLRP3 inflammasome by promoting K(+) efflux. Eur. J. Immunol. *45*, 2927–2936.

Rühl, S., Shkarina, K., Demarco, B., Heilig, R., Santos, J.C., and Broz, P. (2018). ESCRT-dependent membrane repair negatively regulates pyroptosis downstream of GSDMD activation. Science *362*, 956–960.

Santos, J.C., Dick, M.S., Lagrange, B., Degrandi, D., Pfeffer, K., Yamamoto, M., Meunier, E., Pelczar, P., Henry, T., and Broz, P. (2018). LPS targets host guanylate-binding proteins to the bacterial outer membrane for non-canonical inflammasome activation. EMBO J. *37*.

Schrör, K. (1997). Aspirin and platelets: the antiplatelet action of aspirin and its role in thrombosis treatment and prophylaxis. Semin. Thromb. Hemost. *23*, 349–356.

Seymour, C.W., Liu, V.X., Iwashyna, T.J., Brunkhorst, F.M., Rea, T.D., Scherag, A., Rubenfeld, G., Kahn, J.M., Shankar-Hari, M., Singer, M., et al. (2016). Assessment of Clinical Criteria for Sepsis: For the Third International Consensus Definitions for Sepsis and Septic Shock (Sepsis-3). JAMA *315*, 762–774.

Shah, K.G., Wu, R., Jacob, A., Molmenti, E.P., Nicastro, J., Coppa, G.F., and Wang, P. (2012). Recombinant human milk fat globule-EGF factor 8 produces dose-dependent benefits in sepsis. Intensive Care Med. *38*, 128–136.

Shi, J., Zhao, Y., Wang, K., Shi, X., Wang, Y., Huang, H., Zhuang, Y., Cai, T., Wang, F., and Shao, F. (2015). Cleavage of GSDMD by inflammatory caspases determines pyroptotic cell death. Nature *526*, 660–665.

Sun, L., Wang, H., Wang, Z., He, S., Chen, S., Liao, D., Wang, L., Yan, J., Liu, W., Lei, X., and Wang, X. (2012). Mixed lineage kinase domain-like protein mediates necrosis signaling downstream of RIP3 kinase. Cell *148*, 213–227.

Suzuki, J., Umeda, M., Sims, P.J., and Nagata, S. (2010). Calcium-dependent phospholipid scrambling by TMEM16F. Nature *468*, 834–838.

Taylor, F.B., Jr., Toh, C.H., Hoots, W.K., Wada, H., and Levi, M.; Scientific Subcommittee on Disseminated Intravascular Coagulation (DIC) of the International Society on Thrombosis and Haemostasis (ISTH) (2001). Towards definition, clinical and laboratory criteria, and a scoring system for disseminated intravascular coagulation. Thromb. Haemost. *86*, 1327–1330.

van der Poll, T., and Herwald, H. (2014). The coagulation system and its function in early immune defense. Thromb. Haemost. *112*, 640–648.

Vanaja, S.K., Russo, A.J., Behl, B., Banerjee, I., Yankova, M., Deshmukh, S.D., and Rathinam, V.A.K. (2016). Bacterial Outer Membrane Vesicles Mediate Cytosolic Localization of LPS and Caspase-11 Activation. Cell *165*, 1106–1119.

von Moltke, J., Trinidad, N.J., Moayeri, M., Kintzer, A.F., Wang, S.B., van Rooijen, N., Brown, C.R., Krantz, B.A., Leppla, S.H., Gronert, K., and Vance,

R.E. (2012). Rapid induction of inflammatory lipid mediators by the inflammasome in vivo. Nature *490*, 107–111.

Wang, J., and Kubes, P. (2016). A Reservoir of Mature Cavity Macrophages that Can Rapidly Invade Visceral Organs to Affect Tissue Repair. Cell *165*, 668–678.

Wang, Y., Gao, W., Shi, X., Ding, J., Liu, W., He, H., Wang, K., and Shao, F. (2017). Chemotherapy drugs induce pyroptosis through caspase-3 cleavage of a gasdermin. Nature *547*, 99–103.

Wang, S., Miura, M., Jung, Y.K., Zhu, H., Li, E., and Yuan, J. (1998). Murine caspase-11, an ICE-interacting protease, is essential for the activation of ICE. Cell *92*, 501–509.

Watanabe, R., Sakuragi, T., Noji, H., and Nagata, S. (2018). Single-molecule analysis of phospholipid scrambling by TMEM16F. Proc. Natl. Acad. Sci. USA *115*, 3066–3071.

Yang, D., He, Y., Muñoz-Planillo, R., Liu, Q., and Núñez, G. (2015). Caspase-11 Requires the Pannexin-1 Channel and the Purinergic P2X7 Pore to Mediate Pyroptosis and Endotoxic Shock. Immunity *43*, 923–932.

Yang, Z., Wang, Y., Zhang, Y., He, X., Zhong, C.Q., Ni, H., Chen, X., Liang, Y., Wu, J., Zhao, S., et al. (2018). RIP3 targets pyruvate dehydrogenase complex to increase aerobic respiration in TNF-induced necroptosis. Nat. Cell Biol. *20*, 186–197.

Zanoni, I., Tan, Y., Di Gioia, M., Broggi, A., Ruan, J., Shi, J., Donado, C.A., Shao, F., Wu, H., Springstead, J.R., and Kagan, J.C. (2016). An endogenous caspase-11 ligand elicits interleukin-1 release from living dendritic cells. Science *352*, 1232–1236.

Zhang, Y., Meng, H., Ma, R., He, Z., Wu, X., Cao, M., Yao, Z., Zhao, L., Li, T., Deng, R., et al. (2016). Circulating Microparticles, Blood Cells, and Endothelium Induce Procoagulant Activity in Sepsis through Phosphatidylserine Exposure. Shock *45*, 299–307.

STAR★METHODS

KEY RESOURCES TABLE

REAGENT or RESOURCE	SOURCE	IDENTIFIER
Antibodies for Immuno-blot and Immunohistochemisty		
Anti-caspase-11 antibody	Sigma	Cat#: C1354; RRID: AB_258736
Anti-RIP3, antibody	Santa cruz	Cat#: sc-374639; RRID: AB_10992232
Anti-MLKL, antibody	Abcam	Cat#: ab184718; RRID: AB_2755030
Anti-phosphorylated RIP3 antibody	Abcam	Cat#: ab209384; RRID: AB_2714035
Anti- phosphorylated MLKL antibody	Abcam	Cat#: ab187091; RRID: AB_2619685
Anti-GSDME antibody (clone EPR19859)	Abcam	Cat#: ab215191; RRID: AB_2737000
Anti-caspase3 antibody	Cell Signaling Technology	Cat#: 9662S; RRID: AB_331439
Anti-fibrin antibody 59D8	From Nigel Mackman	Hui et al., 1983
Anti-TF antibody (clone EPR8986)	Abcam	Cat#: ab151748
Anti -TMEM16F antibody (ANO6)	Invitrogen	Cat#: PA5-69345; RRID: AB_2691066
β-actin antibody (clone 8H10D10),	Cell Signaling Technologies	Cat#: 3700S; RRID: AB_2242334
1H1 anti-TF antibody	From D. Kirchhofer	Kirchhofer et al., 2005
Antibodies for immunofluorescence		
AF647-labeled anti-mouse CD49b	Biolegend	Cat#: 103511; RRID: AB_528830
Alexa Fluor 647 antibody labeling kits	Invitrogen	Cat#: A20186
Alexa Fluor 555 antibody labeling kits	Invitrogen	Cat#: A20187
5-FAM/QXL-520 FRET thrombin substrate	Anaspec	Cat#: AS-72129
Anti-mouse Albumin antibodies	Bethyl	Cat#: A90-234A; RRID: AB_67122
Anti-mouse fibrin antibody 59D8	provided by Nigel Mackman	Hui et al., 1983
FITC-Annexin-5	BD bioscience	Cat#: 556420
APC-Annexin-5	BioLegend	Cat#: 640920; RRID: AB_2561515
Antibodies for Flow Cytometry		
Bovine Lactadherin - FITC	Haematologic Technologies.	BLAC-FITC
APC anti-humanCD45 (2D1)	BioLegend	Cat#: 368512; RRID: AB_2566372
Chemicals, Peptides, and Recombinant Proteins		
Ultrapure LPS (*E. coli* 0111:B4)	InvivoGen	tlrl-3pelps
Poly(I:C) LMW	InvivoGen	tlrl-picw-250
Cholera Toxin B Subunit (Choleragenoid) from Vibrio cholerae	List Biological Laboratories, INC.	103B
Bovine Lactadherin	Haematologic Technologies.	BLAC-1200
Recombinant Mouse MFG-E8 Protein	R&D systems	2805-MF-050
Lipofectamine RNAiMAX Transfection Reagent	Invitrogen	13778075
Niflumic acid	Sigma-Aldrich	N0630-10 g
Tannic acid	Sigma-Aldrich	V900190-100 g
propidium iodide	Sigma-Aldrich	P4864
Glycine	Sigma-Aldrich	G8898
Peptidoglycan from Staphylococcus aureus	Sigma-Aldrich	77140
Cycloheximide (CHX)	Sigma-Aldrich	C7698
Mouse immunoglobin IgG protein	Abcam	ab198772
Human TNF- α	Invivogen	rcyc-htnfa
BAPTA-AM	Sigma-Aldrich	A1076
zVAD	Selleck	S7023
Smac mimetic (SM-164)	APExBIO	A8815
A23187	Sigma-Aldrich	C9275

(*Continued on next page*)

Continued

REAGENT or RESOURCE	SOURCE	IDENTIFIER
EDTA	Sigma-Aldrich	798681
PGPC	Cayman Chemical	N°10044
Critical Commercial Assay		
LDH Cytotoxicity Assay kit	Beyotime Biotechnology	Cat#: C0016
Human Tissue Factor Chromogenic Activity Kit	Assaypro	Cat#: CT1002b
Human IL-6 Uncoated ELISA	Invitrogen	Cat#: 88-7066; RRID: AB_2574991
Human CRP ELISA	Abcam	Cat#: ab181416
Human IL-1 alpha ELISA	Abcam	Cat#: ab178008
Human IL-1 beta Uncoated ELISA	Invitrogen	Cat#: 88-7261; RRID: AB_2575051
Fibrinogen Mouse ELISA Kit,	Abcam	Cat#: ab108844
PAI-1Mouse Simple Step ELISA Kit,	Abcam	Cat#: ab197752
TAT Complexes Mouse ELISA Kit	Abcam	Cat#: ab137994
Mouse d-dimer (D2D) ELISA Kit	Cloud-Clone	CEA506Mu
Human TAT assay	SEKISUI MEDICAL	30568000
Human PAI-1 assay	SEKISUI MEDICAL	43073000
IL-1α Mouse Uncoated ELISA Kit	Invitrogen	Cat#: 88-5019; RRID: AB_2574807
IL-1β Mouse Uncoated ELISA Kit	Invitrogen	Cat#: 88-7013; RRID: AB_2574946
Experimental Models: Cells		
Mouse Macrophages	Prepared in Lu Lab	Described in current manuscript
GSDMD $^{-/-}$ HeLa cells	Feng Shao Lab	Wang et al., 2017
GSDMD$^{-/-}$ -Flag-GSDME HeLa cells	Feng Shao Lab	Wang et al., 2017
GSDMD $^{-/-}$*CASPASE-3* $^{-/-}$ HeLa cells	Feng Shao Lab	Wang et al., 2017
GSDMD$^{-/-}$ *CASPASE-3*$^{-/-}$-Flag-GSDME HeLa cells	Feng Shao Lab	Wang et al., 2017
Wild-type HT-29 cells	Jiahuai Han Lab	Yang et al., 2018; RRID: CVCL_0320
RIP3$^{-/-}$ HT-29 cells	Jiahuai Han Lab	Yang et al., 2018
MLKL$^{-/-}$HT-29 cells	Jiahuai Han Lab	Described in current manuscript
Experimental Models: Strains		
C57BL/6 mice	Jackson Laboratories	JAX:000664
Casp11$^{-/-}$ mice	Jackson Laboratory.	JAX: 024698
Gsdmd$^{-/-}$ mice	Jiahuai Han Lab	He et al., 2015
P2x7r$^{-/-}$ mice	Jackson Laboratory.	JAX:005576
Il-1r$^{-/-}$ mice	Jackson Laboratory.	JAX: 003245
Tlr4$^{-/-}$ mice	Jackson Laboratory.	JAX: 007227
Low-TF mice (*mTF*$^{-/-}$/*hTF*$^{+}$)	Nigel Mackman Lab	Parry et al.,1998
HCV mice (*HTF*$^{+}$)	Nigel Mackman Lab	Pawlinski et al., 2007
Oligonucleotides		
GCAUACGAAUCUAACCUUATT	This paper	Mouse *Tmem16f*-specific siRNA1
GCGAGAAGAUUGGAAUCUATT	This paper	Mouse *Tmem16f* -specific siRNA2
CCCAAGAACAUUAAUGGAATT	This paper	Human *TMEM16F*-specific siRNA1
CCUGGUCUUUGCAGUAUUUTT	This paper	Human *TMEM16F*-specific siRNA2
UUCUCCGAACGUGUCACGUTT	This paper	Control siRNA
5′-AACCCACCAACTATACCTACACT-3′	PrimerBank	*TF* –specific primers
5′-GTCTGTGAGGTCGCACTCG-3′		
Software and Algorithms		
Graphpad Prism 7 software	Graphpad Prism 7 software	N/A
Adobe Photoshop CS6	Adobe	N/A
NIS Elements software	Nikon Instruments	N/A
ImageJ	NIH	N/A

LEAD CONTACT AND MATERIALS AVAILABILITY

Further information and requests for resources and reagents may be directed to and will be fulfilled by the Lead Contact, Ben Lu (xybenlu@csu.edu.cn).

EXPERIMENTAL MODEL AND SUBJECT DETAILS

Mouse studies

WT C57BL/6J mice, *Casp11*$^{-/-}$ mice, *Tlr4*$^{-/-}$ mice, *Il-1r*$^{-/-}$ mice and *P2x7r*$^{-/-}$ mice on a C57BL/6J background were purchased from Jackson Laboratory. *Gsdmd*$^{-/-}$ mice were a kind gift from Professor Jiahuai Han at the Xiamen University (He et al., 2015). *Low-TF* (*LTF*) mice express very low levels of human (h) TF (approximately 1% relative to mouse [m] TF) and completely lacking mouse TF (*mTF*$^{-/-}$/*hTF*$^{+}$) and WT littermates (*mTF*$^{+/+}$/*hTF*$^{+}$) were used as controls (Parry et al., 1998). *HCV* mice (*mTF*$^{-/-}$/*HTF*$^{+}$) express high levels of human TF (~100% of WT TF levels except in the heart) in the absence of mouse TF from a human chromosome vector (HCV) and the only source of TF is from the HCV (Pawlinski et al., 2007). In order to express high levels of human TF in WT, *Casp11*$^{-/-}$ and *Gsdmd*$^{-/-}$ mice, *HCV* mice were crossed with WT, *Casp11*$^{-/-}$ and *Gsdmd*$^{-/-}$ mice to generate WT (*HTF*$^{+}$), *Casp11*$^{-/-}$ (*HTF*$^{+}$) and *Gsdmd*$^{-/-}$ (*HTF*$^{+}$) mice. All transgenic mice used in our research were confirmed using standard genomic PCR genotyping techniques. Animals were maintained in a specific pathogen-free environment at the Department of Laboratory Animals of Central South University. In the current study, we used WT littermates as the controls for the transgenic mice. All experimental animal protocols were approved by the Institutional Animal Care and Use Committees of Central South University.

LPS-induced Endotoxemia and E.coli-induced peritonitis

For the lethal endotoxin sepsis model, male mice 25 to 30 g in weight were injected intraperitoneally with 0.4 mg/kg LPS or 10 mg/kg poly(I:C) (priming) and then challenged 7 hr later with 10 mg/kg LPS or anti-mouse monoclonal TF neutralizing antibody (Kirchhofer et al., 2005) 1H1(400 μg/mouse) or the control isotype IgG (400 μg/mouse) 30 min before LPS challenged or with or without MFG-E8 (160 μg/kg) 2h before LPS injected. For *E.coli*-induced sepsis, live *E.coli* were grown in LB broth to log-phase, washed, resuspended in sterile saline and then injected intraperitoneally (1 × 10^{9}CFU). Sterile saline was injected intraperitoneally in the control group. In some experiments, low molecular weight heparin (LMWH; Enoxaparin Sodium Injection, Sanofi-Synthelabo Limited, the France) 200IU/kg or sterile saline (control group) was administered subcutaneously 30 min before each LPS or *E.coli* injection. Mice were sacrificed at 8 hr after LPS treatment or 12 hr after injection of *E.coli*. Survival was observed for up to 7days. Mice were euthanized when they became moribund.

Caecal Ligation and Puncture (CLP)

To induce polymicrobial sepsis, CLP was conducted as previously described (Rittirsch et al., 2009). Briefly, the skin was disinfected with a 2% iodine tincture. Laparotomy was performed under 2% isoflurance (Piramal Critical Care) with oxygen. For the sub lethal model, 50% of the cecum was ligated and punctured twice with a 22-gauge needle. Warm saline (1 mL) was given subcutaneously for resuscitation immediately after operation. For the lethal model, 75% of the cecum was ligated and punctured twice with an 18-gauge needle. Mice were sacrificed at 24 hr after CLP. Survival was observed for up to 7days. Mice were euthanized when they became moribund.

Cell lines culture and stimulation

GSDMD$^{-/-}$ HeLa cells, *GSDMD*$^{-/-}$ HeLa cells stably expressing WT GSDME (Flag-GSDME), *GSDMD*$^{-/-}$ *CASP3*$^{-/-}$HeLa cells, *GSDMD*$^{-/-}$ *CASP3*$^{-/-}$ HeLa cells stably expressing WT GSDME (*CASP3*$^{-/-}$-Flag-GSDME) were all obtained from Feng Shao's lab at the National Institute of Biological Sciences of China. Construction of the above cell lines were described previously (Wang et al., 2017). WT, *RIP3*$^{-/-}$and *MLKL*$^{-/-}$ HT-29 cells were obtained from the Dr. Jiahuai Han's lab at the Xiamen University. *RIP3*$^{-/-}$ HT-29 cells were established and described previously (Yang et al., 2018). For generation of *MLKL*$^{-/-}$ HT-29 cells, CRISPR/Cas9 genomic editing for gene deletion was performed according to the previous publication (Yang et al., 2018). Guide RNA sequence targeting human *MLKL* (5′- ggagctctcgctgttacttc-3′) exons was cloned into the plasmid. Single colonies were obtained by serial dilution and amplification. The genome type of the knockout cells was determined by DNA sequencing and western blot. HeLa cells and HT-29 cells were cultivated in Dulbecco's modified Eagle's medium (DMEM) supplemented with 10% (v/v) fetal bovine serum (FBS) and 2mM l-glutamineat 37°C in a humidified incubator containing 5% CO_2. HeLa Cells were stimulated with 20 ng/ml human TNF-α plus 10 μ g/ml cycloheximide for 5 hr. HT-29 cells were treated with TNF-α (T, 30 ng/ml) +Smac (S,1 μM)+ zVAD (Z, 20 μM) for 6 hr. For siRNA silencing of human *TMEM16F*, siRNA were transfected with Lipofectamine RNAiMAX Transfection Reagent into the HeLa cells and HT-29 cells according to the manufacturer's instructions. 48 h after transfection, cells were treated with the above stimuli. The siRNA target sequences are CCCAAGAACAUUAAUGGAATT (si1-*16F*), CCUGGUCUUUGCAGUAUUUTT (si2-*16F*) and UUCUCCGAACGUGUCACGUTT (si-control).The silencing efficiency was examined by qRT-PCR and immunoblot.

Macrophage cultures and stimulation

Mouse peritoneal macrophages were harvested as previously described (Lu et al., 2012). Briefly, 6-8 week mice were injected intraperitoneally with 3 mL of sterile 3% thioglycollate broth to elicit peritoneal macrophages. 72 hr later,cells were collected by peritoneal

lavage with 5mL of RPMI medium 1640 (Hyclone). After washing, harvested cells were resuspended in RPMI-1640 containing 10% fetal bovine serum (GIBCO) and 1% antibiotics (GIBCO). Cells plated in 12-well plates or 24-well plate were stimulated with LPS (1 μg/ml) plus cholera toxin subunit B (CTB, 20 μg/ml) in normal Ca^{2+}-containing medium with or without different concentrations of EDTA (200-600 μM), BAPTA-AM (4-10 μM), lactadherin (100-300 nM), rMFG-E8 (0.01-0.05 μg/ml), mannitol (5-10 mg/ml) and glycine (10mM) or in low Ca^{2+}- containing medium supplemented with or without different concentrations of Ca^{2+} (100-400 μM). Macrophages were incubated with A23187 (2 μM) for 30 min after primed with LPS (1 μg/ml) 6 hr in normal Ca^{2+}-containing medium. In experiments where K^+ efflux was inhibited, increasing concentrations of KCl (50mM) was added to the RPMI medium 1640 at the time of stimulation. To silence the expression of mouse endogenous *Tmem16f*, siRNAs for *Tmem16f* was transfected with Lipofectamine RNAiMAX Transfection Reagent in primary peritoneal macrophages according to the instruction. The sequences of two siRNAs were as follow: siRNA1: 5′-GCAUACGAAUCUAACCUUATT-3′; siRNA2: 5′-GCGAGAAGAUUGGAAUCUATT-3′. To induce the hyperactive state, macrophages were primed with 1 μg/ml LPS for 4 hr, then treated with 100 μg/ml PGPC or 50 μg/ml peptidoglycan (PGN) for 6 hr. The PGPC was supplied as a solution in ethanol. To change the solvent, the ethanol was evaporated under a gentle nitrogen gas stream, leaving only the lipids in the glass vials and pre-warmed serum-free RPMI medium 1640 was immediately added to the dried lipids. The final concentration of PGPC was at 1 mg/ml. Reconstituted lipids were incubated at 37°Cfor 10 mins and were vortexed vigorously for 1 min before added to cells. PGN was resuspended in PBS pH 7.4 at a concentration of 2 mg/ml and vortexed vigorously for 5min before dilution and addition into cells.

Clinical Human Samples

Patients were diagnosed with sepsis first according to the 2016 International Sepsis Definitions (Seymour et al., 2016) and then DIC according to ISTH criteria 2001 (Taylor et al., 2001) (DIC scores were calculated according to International Society on Thrombosis and Hemostasis 2001, "overt" DIC score standard. Exclusion criteria were: age < 18 years, preexisting immunosuppression; transplant recipient; presence of decompensated cirrhosis (Child-Pugh class B or C), hematological diseases, any disease involving hemodialysis such as chronic renal failure, and history of anticoagulant therapy during the preceding four weeks. A total of 51 patients from the intensive care unit (ICU) at the Third Xiangya Hospital of Central South University from September 2017 to October 2018 met the above conditions. The primary endpoint was the development of overt DIC within the first two days of ICU stay. The secondary endpoint was 28-day all-cause mortality. Plasma samples were obtained on days 1 to 2 when these patients were newly diagnosed with sepsis after admission to ICU. Blood sampling was performed as soon as possible (< 6 hr) when all patients fulfilled septic shock criteria to avoid any therapeutic bias. Sampling on ethylene-diamine-tetraacetic acid (1.8 mg/mL) and citrate (0.129 M) anticoagulants was performed at admission. Poor platelet citrated plasma was obtained after a two-step centrifugation (20 min; 3500 g). Plasma samples were stored at −80°C when these patients were newly diagnosed with sepsis after admission. Information about the patients was recorded, especially for overt DIC score on 2 successive days and 28-day mortality (Table S1). Informed consent was conferred by the patients or their families and this study was approved by the research ethics committee of the Third Xiangya Hospital of Central South University (NO. 2017-S209)

METHOD DETAILS

Preparation of the Liver and Lung for Intravital Microscopy

In order to better observe the dynamic changes of liver and lung microcirculation under the confocal intravital microscopy and ensure that most of vessel was not completely occluded, mice were administered 4mg/kg LPS intraperitoneally with or without heparin. Mice were anesthetized with 10 mg/kg xylazine hydrochloride and 200 mg/kg ketamine hydrochloride. Then internal jugular vein catheterization was performed for further injection of drugs and antibodies. Preparation of the mouse liver for intravital microscopy was performed as previously described (Wang and Kubes, 2016). Briefly, a midline incision was made and extended through the thoracic margin to the midaxillary line, then the liver was externalized onto a thin glass coverslip located on the inverted microscope heat-controlled stage with a thermostatic device. The liver was draped with saline-soaked gauze to avoid tissue dehydration and to help limit movement of the liver on the coverslip. Fluorescent images of liver sections from mice were photographed by Spinning Disk Confocal Intravital Microscopy (SD-IVM). Preparation of the lung for imaging in mice with minimal disruption of ventilation or circulation reported before (Lefrançais et al., 2017). Briefly, anesthetized mice were surgically exposed to small areas of the left chest and left lung. The purpose of the surgery is to construct a thoracic window with 5 mm internal diameter. Video and images were collected through a vacuum-chamber with a glass slide that its loose adherence to the exposed left lung surface via negative pressure with 20–25 mm Hg.

Spinning Disk Confocal Intravital Microscopy Analysis

The exposed liver (leftmost lobe of the liver) was visualized with a Nikon Ti2-E inverted microscope (Nikon Instruments) equipped with a Yokogawa CSU-W1 head (Yokogawa Electric Corporation). A Plan Apochromat Lambda 10 × N.A. 0.45 or Plan Apochromat Lambda 20X N.A. 0.75 air objective was used for all experiments. Four laser excitation wavelengths (405, 488, 561 and 640 nm; TOPTICA Photonics) were used in rapid succession and visualized with the appropriate long-pass filters (Semrock and Chroma). Exposure times for excitation wavelengths were 100 ms for all lasers. A scientific complementary metal oxide semiconductor (sCMOS) camera (Prime 95B, Photometrics) was used for fluorescence detection. NIS-Elements AR software (Nikon Instruments) was used to drive the microscope. Anti-mouse Albumin antibodies and anti-mouse Fibrin antibodies (Hui et al., 1983) (provided

by Nigel Mackman) were conjugated to Alexa Fluor 647 or Alexa Fluor 555 antibody labeling kits. Thrombin generation was visualized using SensoLyte internally-quenched 5-FAM/QXL-520 FRET thrombin substrate (2 μL/mouse). Platelets were visualized using AF647-anti-CD49b antibody (5 μL/mouse). Fibrin deposition was visualized using Alexa Fluor 555-conjugated anti-mouse fibrin antibody (4 μL/mouse) and perfused vessels were visualized using Alexa Fluor 647-conjugated anti-mouse albumin antibody (15 μL/mouse). Antibodies were administered via internal jugular vein catheterization 4 min before imaging. Image analysis methodology was performed as previously described (Kolaczkowska et al., 2015). Briefly, images were saved in tiff format, exported and analyzed in ImageJ (NIH). For the elimination of background autofluorescence, contrast was adjusted to minimize autofluorescent background staining, and a minimum brightness threshold was set to emerge only positive staining. Identical contrast and threshold values were applied to all images within our study. Threshold images were converted to binary, and the area per field of view covered by positive fluorescence staining was analyzed through ImageJ software. Data are expressed as the percentage of area in each field of view covered by positive fluorescence staining.

Multiphoton Laser Scanning Confocal Intravital Microscopy Analysis

Images the exposed left lung were acquired with an Olympus multiphoton imaging system (FVMPE-RS, Tokyo, Japan) using a 25x/NA 1.05 water-dipping objective. The microscope system was equipped with a multiphoton light path installed on upright microscope (BX63, Olympus), and a tunable femtosecond pulse laser (MaiTai DeepSee, Spectra Physics, USA). The excitation wavelength was tuned to 920 nm and the emission filters were selected as 495-540nm for green channel and 575-645nm for red channel. Antibodies injection and images analysis were performed as described above.

ELISA, Biochemical Assays and LDH Assay

Blood was drawn by heart puncture in heparinized syringes from anesthetized mice. Plasma was isolated rapidly after high-speed centrifugation (3000 × g, 10 min) at 4°C. Mouse plasma concentrations of TAT, PAI-1, Fib and D-dimer were measured using commercially ELISA kits. To measure tissue MPO activity, lungs were perfused with cold PBS, frozen and stored at −80°C for no more than one week. Mouse serum concentrations of ALT, AST and Crea were detected using an autoanalyzer (Sysmex DRI-CHEM3500, Fuji, Japan). Cell culture supernatant samples were analyzed using IL-1β and IL-1α ELISA Kit and cell death was assessed by LDH Cytotoxicity Assay Kit. Patients plasma samples were assayed with Human IL-1β (minimal detectable dose is 2pg/mL) and IL-1α ELISA (minimal detectable dose is 0.5 pg/mL) Kits according to the instructions.

Liver and Lung Histology

After cardiac perfusion with PBS containing heparin (6.25IU/ml), the right upper lobe of the liver and right upper lobe of lung were fixed in 4% paraformaldehyde and paraffin embedded, then 4 μm thick sections were cut and stained with hematoxylin and eosin; Some other sections were incubated with the primary antibody, rabbit anti-mouse fibrin antibody (1:500) overnight at 4°C.

Tissue factor activity, thrombin and fibrin assays

Cell pro-coagulant activity was assayed using Human Tissue Factor Chromogenic Activity Kit, SensoLyte and AFC Thrombin Activity Assay Kit (Fluorimetric). Macrophages (*HTF*$^{+}$) lysate or plasma of *HCV* mice and patients, were directly added to the assay mix containing FVII and FX and incubated at 37°C 30 min followed by addition of 20 μL FXa substrate. Read the absorbance at 405 nm every 5 min for 25 min and TF concentration was calculated from the Standard Curve. For thrombin generation assay, fresh platelet poor plasma (PPP) was obtained from blood drawn by heart puncture with a sodium citrate anticoagulant syringe from an anesthetized *HCV* mouse. The blood (1-2 ml) was collected and centrifugal (250 × g) at 37°C for 10 min. Transfer supernatant to new tube and then centrifugal (3500 g) for 10 min for two times, the supernatant is PPP. To ensure a uniform background level of cell-stimulated coagulation activation, plasma from several mice was mixed and frozen at −80°C, 10 μL *HCV* macrophages lysate were added to 40 μL diluted PPP (diluted with RPMI 1640 and 10mM $CaCl_2$) with or without 1H1 or argatroban in the 96-well black microplate. Finally, 50 μL thrombin substrate was added, fluorescence intensity was recorded immediately in a kinetic mode according to the instructions of thrombin Activity Assay kit on a TECAN multifunctional fluorescent enzyme-labeled instrument. Fibrin formation was assayed according to the previous method (Cao et al., 2017).

Measurement of PS exposure

PS exposure was detected by flow cytometry and immunofluorescence. Mice splenic cells and peripheral blood cells were stained with lactadherin-FITC (16nM) 30 min in the dark and analyzed on the Arai-II-Flow Cytometer (BD Biosciences). PS exposure on the surface of macropahges or other cells plated on six- well slide was visualized by staining with Annexin V-FITC or Annexin V-APC. The images of fluorescently stained cells were captured with the high content screening system ScanR (Olympus) and the methods of image capture and analysis were referred to previous reports (Risom et al., 2018). Briefly, the z stack images were acquired by Olympus spinSR system with 40 × objective lens (NA0.95), and then analyzed by Olympus ScanR Analysis Software. Single-cell nuclear and the cell membrane fluorescent intensities were calculated using the Olympus ScanR Analysis Software: the DAPI-positive region of each cell was used to do the segmentation and quantitate the cell number, and a 20 pixelannulus around the nucleus was used to quantitate cytoplasmic signal, omitting the nuclear signal.

Immunoblot analysis and qRT–PCR

Cells and tissue lysates were prepared. Protein samples were separated by 10% or 12% SDS-PAGE and transferred onto PVDF membranes (Millipore). Antibodies to TF, TMEM16F, RIP3, MLKL, phosphorylated RIP3, phosphorylated MLKL, CASPASE-3 and GSDME were used at 1:1000 dilution. Blots were normalized to β-actin expression (1:5000 dilution). qRT–PCR was performed according to the qRT-PCR kit instruction. The mRNA level of target genes was normalized to that of GAPDH.

QUANTIFICATION AND STATISTICAL ANALYSIS

Statistical calculations were performed with GraphPad Prism7.0 and all data were presented as mean ± SEM. Data were analyzed using 2-tailed Student's t test (for parametric data) or Mann-Whitney U test (for non-parametric data) to determine the significance between population means when two groups were compared. For comparison of more than two groups, 1-way ANOVA or 2-way ANOVA were used with Bonferroni's multiple comparison test. Comparisons between proportions were made using the χ^2 test. In correlation analysis, Pearson's correlation coefficient was calculated. A multivariate statistical analysis called principal component analysis (PCA) was applied to assess the correlation between GSDMD activation and coagulation, or between global inflammation and coagulation. Principal component analysis was applied after standardization as described previously (Jolliffe and Cadima, 2016). In choosing the components, we fixed the number of components to 2. (principal component 1 and principal component 2). Survival studies were analyzed using log-rank test. Values of $p < 0.05$ were considered as statistical significance.

DATA AND CODE AVAILABILITY

The study did not generate datasets/code.